6-2019

AGES OF PREHISTORIC EARTHQUAKES ON THE BANNING STRAND OF THE SAN ANDREAS FAULT, NEAR NORTH PALM SPRINGS, CALIFORNIA

Bryan Castillo
CSUSAN BERNARDINO, bryan.castillo@csusb.edu

AGES OF PREHISTORIC EARTHQUAKES ON THE BANNING STRAND OF THE SAN ANDREAS FAULT, NEAR NORTH PALM SPRINGS, CALIFORNIA

A Thesis

Presented to the

Faculty of

California State University,

San Bernardino

In Partial Fulfillment

of the Requirements for the Degree

Master of Science

in

Earth and Environmental Sciences

---

by

Bryan Adriel Castillo

June 2019

AGES OF PREHISTORIC EARTHQUAKES ON THE BANNING STRAND OF THE SAN ANDREAS FAULT, NEAR NORTH PALM SPRINGS, CALIFORNIA

A Thesis

Presented to the

Faculty of

California State University,

San Bernardino

---

by

Bryan Adriel Castillo

June 2019

Approved by:

Sally F. McGill, Committee Chair, Geological Sciences

Kerry D. Cato, Committee Member, Geological Sciences

Katherine M. Scharer, Committee Member, U.S. Geological Survey

ABSTRACT

We studied a paleoseismic trench that was excavated across the Banning strand of the San Andreas Fault by Petra Geosciences (33.9172°, -116.538°). The trench exposed a ~40 m wide fault zone in interbedded alluvial sand gravel, silt and clay deposits. We present the first paleoseismic record for the Banning strand of the southern San Andreas Fault. The most recent event occurred sometime between 730 and 950 cal BP, potentially coincident with rupture of the San Gorgonio Pass thrust. We interpret that five earthquakes have occurred since 3.3-2.5 ka and eight earthquakes have likely occurred since 7.1-5.7 ka. It is possible that additional events may have occurred without being recognized, especially in the deeper section the stratigraphy, which was not fully exposed across the fault zone. We calculate an average recurrence interval of 380 - 640 yrs based on four complete earthquake cycles between earthquakes 1 and 5. The average recurrence interval is thus equivalent to or less than the elapsed time since the most recent event on the Banning strand. The recurrence interval is similar to the San Gorgonio Pass (450-1850 years) but longer than that for the Mission Creek strand (~220 years).

ACKNOWLEDGEMENTS

I would like to thank my graduate advisor, Dr. Sally McGill for all of her help, insight, and continuous assistance with the process of research and writing of this thesis. I could not have completed a successful thesis without her guidance and mentorship. I would also like to thank my committee members, Dr. Katherine Scharer (USGS) and Dr. Kerry Cato for all of their academic support and insight. Without funding from the USGS, this work would not have been possible.

I would like to give a very special thanks to Alan Pace (Petra Geosciences) for allowing me to take on this project and John Rogers (property owner) for allowing us to work on his property. I would also like to thank Dr. Doug Yule (CSUN) who served as an advisor and a mentor. A big thank you to Devin McPhillips (USGS), James McNeil (CSUN), and all the CSUN and CSUSB students who went out to assist me with field work. All that work would not have been possible without you guys. Finally, I would like to thank my parents for their continuous support throughout this journey, to my roommate/colleague Jose Mora and all my friends that have helped me throughout these tough times.

TABLE OF CONTENTS

LIST OF TABLES

LIST OF FIGURES

CHAPTER ONE

INTRODUCTION

The San Andreas Fault is the longest (~1300 km) and has the highest slip rate of all the faults in California. The northern section of the fault ruptured in 1906, and the south-central section ruptured in 1857. Only the southernmost section of the SAF (SSAF) has not ruptured during the historical record, and current estimates place the most recent rupture in 1726 A.D. ± 7 years (Rockwell et al., 2018).

The SSAF is one of the most complex sections of the fault. From its southern end, the SSAF can be seen as a single right-lateral strike slip strand (the Mission Creek strand) but becomes much more complex towards the northwest. Near Indio, the Banning strand diverges from the Mission Creek strand (Figure 1), and farther to the northwest, the Garnet Hill strand diverges from the Banning strand. In the San Gorgonio pass region, the SAF comprises an intricate network of right-lateral, thrust and reverse faults (Allen,1957; Matti and Morton, 1993, Yule and Sieh (2003)). None of these strands have ruptured in a major earthquake during the period of historical record suggesting a high hazard for a large earthquake on the SSAF.

The distribution of slip among various strands of the SSAF is not well known. The Mission Creek strand seems to accommodate the majority of the

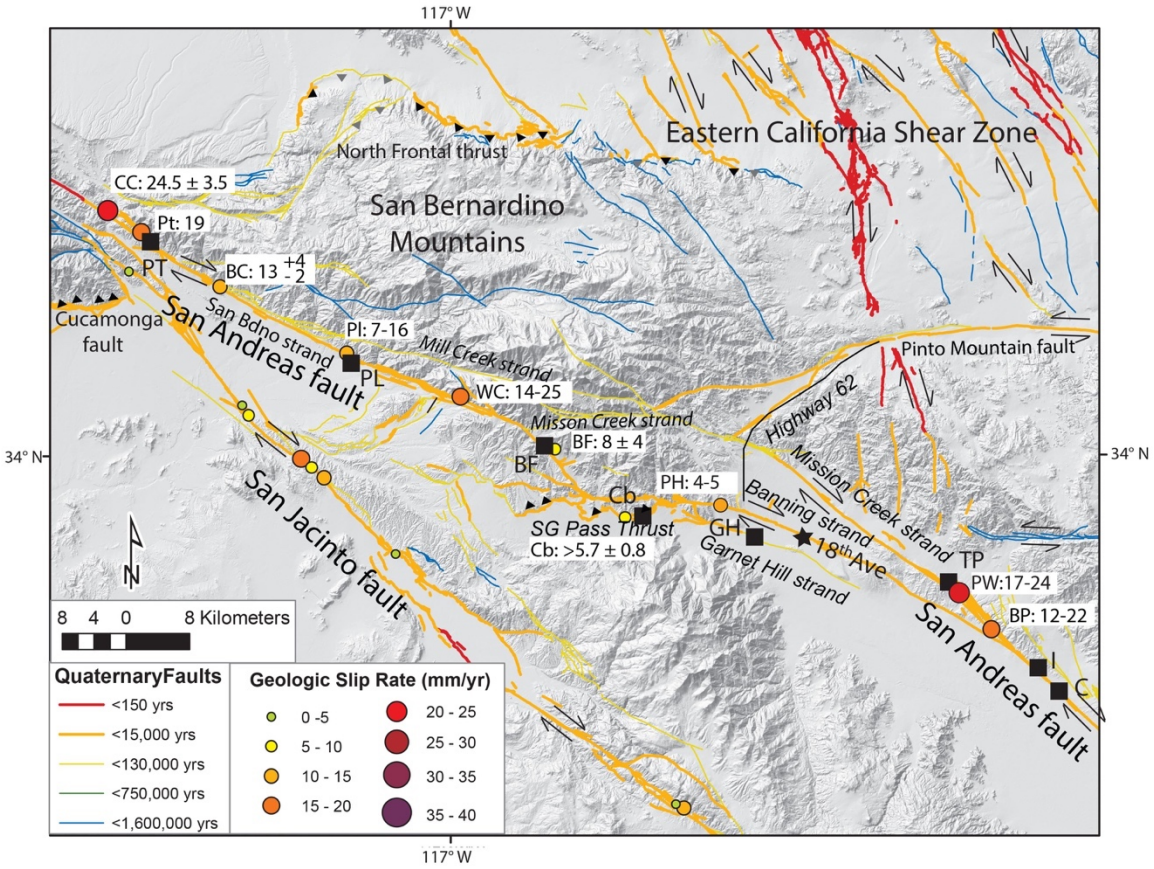

Figure 1. *Quaternary Fault Map of the Greater San Gorgonio Pass Region in Southern California (modified from McGill et al., 2015). Quaternary faults from USGS (2006). Black star shows the location of the 18th Avenue paleoseismic site on the Banning strand of the SSAF. Black squares mark the locations of other paleoseismic sites mentioned in the text (C, Coachella, Philibosian et al., 2011; I, Indio, Sieh and Williams, 1990; TP, Thousand Palms, Fumal et al., 2002a; GH, Garnet Hill, Cardona, 2016; Cb, Cabazon, Scharer et al., 2013; Wolff et al., 2014; BF, Burro Flats, Yule et al., 2007; PL, Plunge Creek, McGill et al., 2002; PT, Pitman Canyon, Seitz et al., 1997). The Wrightwood (Fumal et al., 1993; Fumal et al., 2002b) and Pallet Creek (Scharer et al., 2011) paleoseismic sites are located off the map to the northwest. For context slip rate measurements for the southern San Andreas fault are also shown (colored circles). BC, Badger Canyon (McGill et al., 2016); BF, Burro Flats (Orozco, 2004; Orozco and Yule, 2003); BP: Biskra Palms (Behr et al., 2010; Fletcher et al., 2010; see also van der Woerd et al., 2006); Cb, Cabazon (Yule et al., 2001); CC: Cajon Creek, Weldon and Sieh (1985); PL: Plunge Creek (McGill et al., 2013); Pt: Pitman Canyon (McGill et al., 2016); PW: Pushawalla Canyon (Blisniuk et al., 2012, 2013); WC: Wilson Creek (Harden and Matti, 1989); PH: Painted Hill (Gold et al., 2015).*

slip: the slip rate at Biskra Palms is 12-22 mm/yr (Behr et al., 2010; Fletcher et al., 2010) and at Pushawalla Canyon is 17-24 mm/yr (Blisniuk et al., 2012; Blisniuk et al., 2013). The Banning fault has a slip rate of 2-6 mm/yr in the Indio Hills (Scharer et al., 2016), and 4-5 mm/yr at Painted Hills, near Whitewater (Gold et. al., 2015). No slip rate estimates are available for the Garnet Hill fault, but it is thought to be an active right-lateral fault based on the presence of uplifted areas where there is a series of left-stepovers in the fault (Yule and Sieh 2003; Cardona, 2016).

Although the Mission Creek strand appears to have the highest slip rate of the fault strands in the Coachella Valley, Holocene slip on this fault strand does not appear to continue more than a few km northwest of Highway 62 (Figure 1). Rather, slip on the Mission Creek strand may transfer northward to the Eastern California Shear zone (Nur et al., 1993; Rymer, 1997; Gold et al., 2015), as suggested by modeling of geodetic data (Meade and Hager, 2005; McCaffrey, 2005; Spinler et al., 2010; McGill et al., 2015). Slip on the Banning and Garnet Hill strands likely transfers to the San Gorgonio Pass thrust, which in turn, transfers slip to the San Bernardino strand (Yule and Sieh, 2003) (Figure 1).

To better understand the seismic behavior of the SSAF, the temporal behavior of these five strands (the Mission Creek, Banning, Garnet Hill, and San Bernardino strands, as well as the San Gorgonio Pass thrust) must be examined, including the dates of paleoearthquakes on each strand. Just south of the juncture of the first three of these strands in the Coachella Valley, Philibosian

et al. (2011) found evidence of 5-7 paleoearthquakes in the last ~1100 years at the Coachella site (Figure 1). The average recurrence interval was calculated to be 116-221 years with the most recent earthquake (MRE) occurring in A.D. 1657-1713. Four to five paleoearthquakes were documented by Fumal et al. (2002a) at a trench that was excavated on the Mission Creek strand near Thousand Palms (north of the juncture of the three stands), with the most recent event occurring in A.D. 1520-1680. The ages of the MRE at the Coachella and Thousand Palms sites correlate well with a previous age estimate of A.D. 1703 ±35 for the most recent earthquake on the SSAF near Indio reported by Sieh and Williams (1990). More recent work by Rockwell et al. (2018) suggest that the age of the MRE for the Coachella section and the Mission Creek segment is A.D. 1726 ±7 years. The Garnet Hill strand has no evidence of surface rupture in the last ~600 years (Cardona, 2016). For the San Gorgonio Pass Thrust, 4 to 5 earthquakes have been documented in the last ~6000 years, with the most recent event occurring 630-750 years BP (Wolff, 2018). The recurrence interval was calculated to be 450-1850 years which is significantly longer than at any of the paleoseismic sites on the Mission Creek strand. Yule et al. (2007) documented 9 paleoearthquakes in the last ~2000 years at Burro Flats (Figure 1) on the San Bernardino strand. The average recurrence interval was calculated to be ~300 years with the most recent event inferred to have occurred in 1812 (Yule et. al., 2006).

Two significant historical earthquakes have occurred near the Banning strand of the San Andreas fault: the 1986 M 6.1 North Palm Springs earthquake

and the 1948 M 6.3 Desert Hot Springs earthquake. Aftershocks of the 1986 event define a nearly planar surface that strikes about N60 to 70W, is about 15 km in length, dips northeast and projects to the surface near the Banning fault trace (Nicholson, 1996). The first-motion focal mechanism for the mainshock indicates pure right lateral slip (Nicholson, 1996). Aftershocks of the 1948 event define a plane that strikes N55W, dips steeply 60° to 70°, is about 15-km long and projects to the surface near the trace of the Banning fault near northern Indio Hills. This event was also predominantly right lateral in slip based on its focal mechanisms (Nicholson, 1996). From this, Nicholson (1996) proposes that the Banning fault is nonvertical, is likely segmented according to fault dip, as well as fault strike, and has been the primary source of both of these recent, moderate-sized earthquakes in the Coachella Valley.

The 1986 earthquake did produce up to 9 mm of right-lateral triggered slip 44-86 km southeast of the epicenter along the SSAF (Williams et al., 1988). It also produced some ground cracking on the Banning strand between Whitewater River and Highway 62 but it was concluded these formed due to strong shaking and not actual surface rupture (Sharp et al., 1986). The 1948 earthquake was very similar to the 1986 earthquake in that they were both initiated at depth, propagated bilaterally and did not break the surface (Nicholson, 1996).

There is no age control available for any large prehistoric earthquakes on the Banning strand. Therefore, we have conducted a detailed paleoseismic investigation to understand the timing of prehistoric surface-rupturing

earthquakes on the Banning strand of the San Andreas Fault in the northern Coachella Valley. We report here: 1) the constrained ages eight recent paleoearthquakes; 2) the recurrence interval between earthquakes on this strand; and 3) a comparison of the timing of paleoearthquakes on the Banning strand with those on the San Gorgonio Pass thrust and Mission Creek strand of the San Andreas fault.

CHAPTER TWO

SITE DESCRIPTION

Petra Geosciences excavated a paleoseismic trench (33.9172°, -116.538°) on the Banning strand of the San Andreas Fault at 18th Avenue, in North Palm Springs, California. The purpose of the trench was to determine the precise location of Holocene fault strands for the landowners prior to development of the site as required by the Alquist-Priolo Act of 1972. The lead consultant on the trench invited us to conduct a more detailed paleoseismic study on the open trench. The trench was ~92 m long, ~8 m deep, ~9 m wide at the base and 22 m wide at the top and was located on the flood plain of Mission Creek. At the northern end of the trench a ~40m wide fault zone in was exposed in interbedded bouldery cobble, sand, silt and clay deposits.

The trench was located on the flood plain of Mission Creek, which slopes gently to the south. The trench displayed a ~40m wide fault zone, with down-to-the-north separation across most strands, except for down-to-the-south displacement along the strands at the very northern end of the trench. The fault geometry created a graben at the northern end of the trench, in which 1- to 10-cm-thick layers of very fine sand, silt and clay were deposited, interlayered with deposits of course sand and granules. Some of these fine grained layers extended outside of the graben toward the south, but eventually pinched out. This graben may have formed as a result of a small right step-over in the

Banning strand (Figure 2). South of the fault zone, the trench was dominated by coarse sand and gravel (~10-30 cm) and fine grained layers were absent. A few layers contained boulders up to 0.5 m in diameter. Overall the stratigraphy was good, with distinct and abrupt contacts between layers and consistent lateral continuity along the trench wall. However, because the trench was so wide (9 m wide at the base and 22 m wide at the top), correlation of strata between the west and east walls of the trench was only possible for a few prominent layers.

Faults were present at the northern end of the trench, and it is uncertain whether the trench captured the entire fault zone. A fiber optic line prevented mechanical excavation of the trench any farther north. However, manual hand excavations were conducted to extend the trench exposures several meters farther north. These hand excavations revealed faults with down-to-the-south vertical separation (at ~9 m distance along the east wall and at ~7 m on the west wall), revealing the north side of the graben (Figure 3, Plate 1). This suggests that the trench exposures crossed the main fault zone (the graben area), but it is quite possible that additional minor fault strands are present farther north. Furthermore, the depth of the base of the trench at the center of the graben was only 3 m below the surface on the east wall and only 2 m below the surface on the west wall, compared to the ~ 7 m depth of the trench farther south. Therefore, only the top portion of the stratigraphic section is exposed within the main fault zone.

Figure 2. *LiDAR Image of the Banning Fault. This figure displays the right stepover on the Banning Fault. Dotted black rectangle shows outline of trench.*

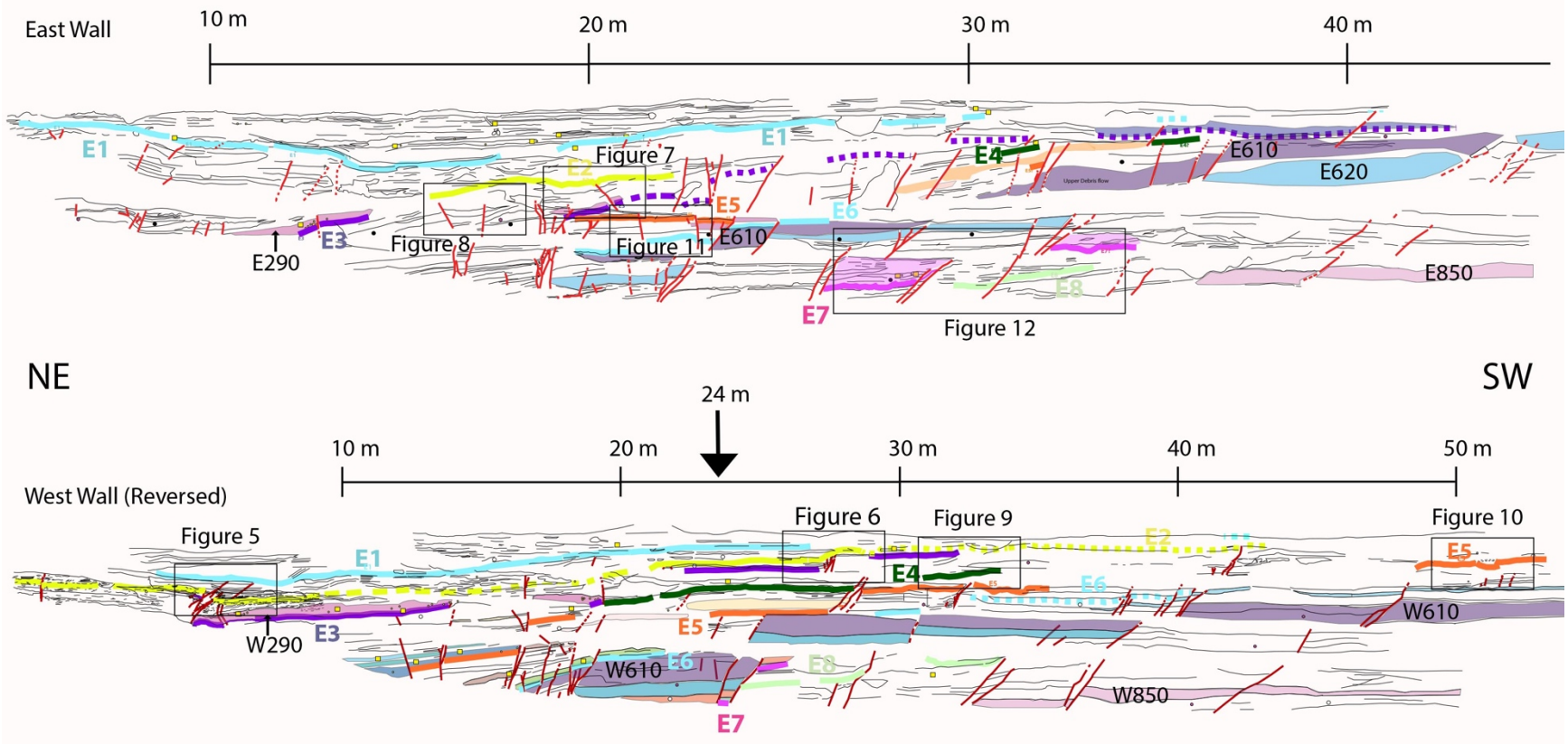

Figure 3. *Cross Section of the Trench Walls. No vertical exaggeration. Selected layers that can be followed for some distance are shaded. The four layers than can be correlated between the two walls of the trench are labeled (290, 610, 620 and 850). Colored, sub-horizontal lines mark the earthquake horizons. Open rectangles show locations of figures 5-12 within the trench.*

CHAPTER THREE

METHODOLOGY

Field Work

Both the east and west walls of the trench had four vertical tiers (each about ~1.5 m high) separated by 3 horizontal benches (each about ~1.5 m in width). We used structure from motion photogrammetric techniques to produce a scaled photomosaic and log of the trench (Figure 3). Absolute reference frame and scale were achieved through surveying with total station a grid of white nails placed approximately 2 m apart along the top and base of each tier. From over 1000 photos, about 500 were used to construct a series of preliminary photomosaics. These photomosaics provided a base for logging and interpretation of stratigraphic layers and faulting in the field. The final orthomosaic was rectified using the surveyed nails as control points.

Recognition of Earthquake Horizons

A central challenge of a paleoseismic investigation is to locate the horizons that were at the ground surface at the times of prehistoric earthquake ruptures on the fault. Upward termination of fault strands is one type of evidence for an earthquake horizon. However, mere upward termination of fault strands is not always a reliable indicator of the stratigraphic position of an earthquake

horizon, because fault strands with small displacements may not necessarily have ruptured all the way to the ground surface at the time of an event (Bonilla and Lienkaemper, 1991). Earthquake horizons are considered more reliable if a sedimentary response to the displacement is preserved (Scharer et al., 2017). For example, when a graben or uphill-facing fault scarp is formed, it may create a closed depression where water will flow and come to a halt depositing very fine grained material in the depression. The fault scarp is preserved and buried by these fine-grained sediments, which generally thin and pinch out at the edges of the depression that formed as result of fault slip at the surface. Thus, both the fault strand and the subsequent depositional record provide more robust evidence of the paleoearthquake horizon than the upward termination alone.

At the 18th Avenue trench, most of the exposed fault strands were located south of the graben and had displacement down to the north. Given the southward slope of the floodplain of Mission Creek, the down to the north displacement during earthquakes created an uphill facing scarp, which caused ponding of fine-grained sediments against it. The southward (and in some cases northward) pinch out of fine-grained layers that filled fault-bounded depressions provided strong evidence for some earthquake horizons.

Radiocarbon Dating

A total of 56 charcoal samples were collected from strata exposed within the 18th Avenue trench, mostly from fine-grained layers. Thirty-three of these

samples have been radiocarbon dated at Lawrence Livermore laboratory to constrain the ages of the prehistoric earthquake horizons. We used the on-line software OxCal (Bronk Ramsey, 2009) with the IntCal 13 calibration curve (Reimer et al., 2013) to calibrate radiocarbon measurements. Results are listed in Table 1.

Luminescence Dating

A total of twenty samples were collected for Infrared Stimulated Luminescence (IRSL) dating. Seventeen of the twenty luminescence samples were prepared and measured at the UCLA Luminescence Lab using a post-IR IRSL protocol (Buylaert et al., 2009) to measure the equivalent dose (De) values for individual grains. Post-IR IRSL225 ages were calculated in the DRAC 1.2 online calculator (Durcan et al., 2015). Age ± 1σ uncertainty is used to report all the luminescence ages (Table 2). Details of the luminescence dating methods used are given in Appendix A.

Table 1. Radiocarbon Dates

CAMS #	Original Sample Name	Strat C. Sample Name	$\delta^{13}C$	fraction Modern	±	$D^{14}C$	±	^{14}C age	±	Calibrated Ages (BC/AD) From	to	%	Calibrated Ages (BP) From	to	Sample Location	Tier	Meter
176783	BF18-46	A46	-25	0.8731	0.0105	-126.9	10.5	1090	100	693	1155	95.4	1257	795	East Wall	1	29.2
176781	BF18-29	A29	-25	0.9708	0.0038	-29.2	3.8	240	35	1522	...	95.4	428	...	East Wall	1	17.3
176782	BF18-47	A47	-25	0.8741	0.0046	-125.9	4.6	1080	45	779	1030	95.4	1171	920	East Wall	1	29.5
177821	B18-B09	B09	-21.3	0.8853	0.0026	-114.7	2.6	980	25	996	1154	95.4	954	796	East Wall	1	9
177818	B18-B07	B07	-24.2	0.8606	0.0038	-139.4	3.8	1205	40	688	945	95.4	1262	1005	East Wall	1	19
177819	B18-B03	B03	-22.5	0.8956	0.0026	-104.4	2.6	885	25	1045	1218	95.4	905	732	East Wall	1	15
177820	B18-B04	B04	-25.7	1.0921	0.0032	92.1	3.2	>Modern		1896	1904	95.4	54	46	East Wall	1	18
176784	BF18-55	A55	-25	0.8602	0.0033	-139.8	3.3	1210	35	689	938	95.4	1261	1012	East Wall	1	20.4
176785	BF18-25	A25	-25.5	0.9201	0.0027	-79.9	2.7	670	25	1276	1390	95.4	674	560	West Wall	1	20.5
176786	BF18-30	A30	-24.2	0.8832	0.0027	-116.8	2.7	1000	25	987	1149	95.4	963	801	East Wall	1	19.3
176787	BF18-53	A53	-25	0.7773	0.0043	-222.7	4.3	2025	45	-165	66	95.4	2115	1884	West Wall	1	29
176788	BF18-11	A11	-22.7	0.7258	0.0024	-274.2	2.4	2575	30	-811	-569	95.4	2761	2519	West Wall	3	9.8
176789	BF18-14	A14	-24.0	0.7238	0.0024	-276.2	2.4	2595	30	-825	-599	95.4	2775	2549	West Wall	3	13
176790	BF18-49	A49	-24.2	0.7265	0.0025	-273.5	2.5	2565	30	-806	-556	95.5	2756	2506	East Wall	3	14.5
176791	BF18-16	A16	-25.4	0.7328	0.0022	-267.2	2.2	2495	25	-773	-540	95.4	2723	2490	West Wall	3	15
177825	B18-B12	B12	-23.9	0.7334	0.0023	-266.6	2.3	2490	30	-781	-511	95.4	2731	2461	East Wall	3	14
176792	BF18-44	A44	-22.6	0.7948	0.0021	-205.2	2.1	1845	25	87	238	95.4	1863	1712	West Wall	2	23.5
177826	B18-C10	C10	-25.0	0.6357	0.0020	-364.3	2.0	3640	25	-2130	-1926	95.4	4080	3876	East Wall	2	32.5
176793	BF18-18	A18	-25	0.7341	0.0051	-265.9	5.1	2480	60	-777	-416	95.4	2727	2366	West Wall	3	20
176794	BF18-39	A39	-25	0.6170	0.0026	-383.0	2.6	3880	35	-2469	-2212	95.4	4419	4162	West Wall	4	16
177829	BF18-33	A33	-25	0.6207	0.0025	-379.3	2.5	3830	35	-2457	-2150	95.4	4407	4100	West Wall	4	18
177830	BF18-35	A35	-20.6	0.6082	0.0019	-391.8	1.9	3995	30	-2576	-2467	95.4	4526	4417	West Wall	4	19.5
177849	BF 18-24	A24	-25	0.5826	0.0027	-417.4	2.7	4340	40	-3086	-2890	95.4	5036	4840	West Wall	4	20.5
177833	B18-C14	C14	-24.0	0.4176	0.0016	-582.4	1.6	7015	30	-5987	-5840	95.4	7937	7790	West Wall	4	23
176795	BF18-21	A21	-25	0.2932	0.0040	-706.8	4.0	9860	120	-9859	-8855	95.4	11809	10805	East Wall	4	31
177834	B18-C12	C12	-22.7	0.3030	0.0009	-697.0	0.9	9590	25	-9151	-8823	95.4	11101	10773	East Wall	4	32.5

Table 1 (Continued)

CAMS #	Original Sample Name	Strat C. Sample Name	$\delta^{13}C$	fraction Modern	±	$D^{14}C$	±	^{14}C age	±	Calibrated Ages (BC/AD) From	to	%	Calibrated Ages (BP) From	to	Sample Location	Tier	Meter
176796	BF18-31	A31	-25	0.2885	0.0299	-711.5	29.9	9990	840	-11810	-7519	95.4	13760	9469	West Wall	4	34
177822	B18-B18	B18	-25	0.7723	0.0049	-227.7	4.9	2080	60	-352	55	95.4	2302	1895	East Wall	2	
177823	B18-C01	C01	-26.7	0.7833	0.0023	-216.7	2.3	1960	25	-38	115	95.4	1988	1835			
177824	BF18-57	A57	-21.9	0.7244	0.0021	-275.6	2.1	2590	25	-811	-767	95.4	2761	2717	East Wall	3	
177827	B18-B11	B11	-23.7	0.6371	0.0022	-362.9	2.2	3620	30	-2118	-1984	95.4	4068	3934	East Wall	3B	
177828	B18-B10	B10	-25	0.6381	0.0026	-361.9	2.6	3610	35	-2120	-1885	95.4	4070	3835	East Wall	3B	
177831	B18-B16	B16	-22.0	0.6201	0.0019	-379.9	1.9	3840	25	-2456	-2203	95.4	4406	4153	East Wall	3	
177832	B18-B17	B17	-25	0.6226	0.0026	-377.4	2.6	3805	35	-2435	-2136	95.4	4385	4086	East Wall	3	

1) $d^{13}C$ values are the assumed values according to Stuiver and Polach (Radiocarbon, v. 19, p.355, 1977) when given without decimal places. Values measured for the material itself are given with a single decimal place. Samples with an (*) were large enough, and as requested to take a sample specific split for IRMS d13C analysis.
2) The quoted age is in radiocarbon years using the Libby half life of 5568 years and following the conventions of Stuiver and Polach (ibid.).
3) Radiocarbon concentration is given as fraction Modern, $D^{14}C$, and conventional radiocarbon age.
4) Sample preparation backgrounds have been subtracted, based on measurements of samples of ^{14}C-free coal. Backgrounds were scaled relative to sample size.
5) CAMS# 176783 and 176795 are <30µg C samples.
6) Error is large on 176796 in part due to the age of sample (nearly two half lives), even though the target was 110µgC

Table 2. Dose-Rate Information and Post-IR IRSL Ages

Lab code	Field code	Unit	Depth (m)	K (%) [a]	Th (ppm) [a]	U (ppm) [a]	Measured gamma dose-rate (Gy/ka) [b]			Total dose-rate (Gy/ka)			Equivalent dose (Gy)			Uncorrected post-IR IRSL age (ka) [c]		
J1284	L01 (BF17-01)	W570	3.8	2.8	19.2	3.28	1.993	±	0.004	6.01	±	0.2	21.69	±	2.2	3.61	±	0.4
J1285	L02 (BF17-02)	W670	4.9	2.7	18.1	2.56	1.897	±	0.004	5.47	±	0.18	29.29	±	2.15	5.36	±	0.45
J1286	L03 (BF17-03)	E690	5.1	2.7	16.3	2.65	1.709	±	0.004	5.04	±	0.17	31.82	±	1.16	6.32	±	0.35
J1287	L04 (BF17-04)	E630	3.5	2.8	15.9	2.57	1.944	±	0.005	5.49	±	0.18	28.31	±	3.6	5.16	±	0.69
J1288	L05 (BF17-05)	E510	2.6	2.7	21.6	2.78	2.458	±	0.005	6.37	±	0.2	31.93	±	1.76	5.01	±	0.35
J1289	L06 (BF17-06)	W320	2.9	2.7	17.3	2.46	1.925	±	0.004	5.69	±	0.19	13.12	±	1.78	2.31	±	0.33
J1290	L07 (BF17-07)	W540C	3.2	2.8	18.7	2.97	1.931	±	0.004	5.9	±	0.19	17.19	±	1.71	2.91	±	0.32
J1291	L08 (BF17-08)	W82B	0.8	2.7	18.5	2.44	1.891	±	0.004	5.7	±	0.19	4.04	±	0.69	0.71	±	0.13
J1292	L09 (BF17-09)	E40	0.8	2.9	15.1	2.51	1.716	±	0.004	5.07	±	0.18	4.29	±	0.51	0.85	±	0.11
J1293	L10 (BF17-10)	W860	6	2.6	19.3	2.46	1.946	±	0.004	5.54	±	0.18	39	±	3.12	7.04	±	0.64
J1294	L11 (BF17-11)	E260	3	2.8	13.8	2.02	N/A	±	N/A	5.21	±	0.18	9.84	±	0.57	1.89	±	0.14
J1394	L15 (BF17-15)	W150E	0.8	2.5	16.1	2.17	1.922	±	0.005	4.88	±	0.17	6.59	±	1.03	1.35	±	0.22
J1395	L16 (BF17-16)	W220E	1.3	2.8	18.3	2.91	1.874	±	0.004	5.9	±	0.19	9.82	±	1.18	1.66	±	0.21
J1396	L17 (BF17-17)	W602C	2.4	2.3	16.9	2.73	2.004	±	0.005	5.52	±	0.17	28.37	±	2.84	5.14	±	0.56
J1397	L18 (BF17-18)	W610	4	2.5	16.3	2.09	1.971	±	0.005	5.05	±	0.17	28.74	±	3.04	5.69	±	0.64
J1398	L19 (BF17-19)	E525	3.6	2.5	17.5	2.71	2.111	±	0.005	5.08	±	0.17	20.55	±	2.78	4.04	±	0.57
J1399	L20 (BF17-20)	E620	3.7	2.4	17.4	2.71	1.89	±	0.005	5.3	±	0.17	26.03	±	2.94	4.91	±	0.59

Location: 33.9174 E, 116.5389 W, 247 m asl.

Grain size used 175-200 μm.

Radionuclide conversion factor after Liritzis et al., 2013; α attenuation factor after Brennan et al., 1991; β attenuation factor after Guerin et al., 2012. Internal K contents were 12.5±0.5% after Huntley and Baril 1997.

Cosmic dose rates following Prescott and Hutton (1994).

U, Th and K contents derived via ICP-MS with relative uncertainties of 5%.

Gamma dose rate derived from *in-situ* gamma spectrometry.

Ages are calculated in DRAC-calculator (Durcan et al., 2015).

Event Quality Rankings

At the 18th Avenue trench, we found evidence for eight paleoearthquake events with varying quality. To compare the strength of evidence for the different events, we use a quality ranking scale to classify each of the indicators for a given event based on the quality of structural and sedimentological evidence that can be used to identify the stratigraphic level that was at the ground surface at the time of the event. Each event indicator is given a quality rank on a scale of 0 to 5 with higher numbers indicating stronger evidence (Table 3).

Table 3 was developed based on a previously published table (Scharer et al., 2017), with a number of additions and clarifications that tailor the criteria to the 18th Avenue trench: (1) It is common for faults that slipped with minor displacement in the same event to terminate upwards at different stratigraphic levels because some of the strands did not rupture all the way to the surface (Bonilla and Lienkaemper, 1991; Weldon et al., 2002). Because of this, Scharer et al., (2017) made a distinction between faults with minor versus moderate offset, with the latter being viewed as more likely to have ruptured to the ground surface thus meriting a higher quality ranking. We choose to classify faults as having “moderate” offset if there is ≥ 5 cm vertical separation, or if the lateral slip is large enough to make correlation of units across the fault uncertain. There is no single number that could be selected for this value that would always distinguish between faults that ruptured to the ground surface and those that did not.

Table 3. Description of Event Indicators and Associated Quality Ranking

Quality	Description
0	- Fault tip where upward termination not distinct due to unclear stratigraphy, resulting in uncertainty as to in which event this fault slipped, with no preferred event horizon among the possibilities. - Fault tip with distinct upward termination, but it remains unclear which event the fault is associated with, because the fault terminates upward at a scoured contact that erodes though one or more event horizons.
1	- Fault with minor offset (<5 cm), even if the upward termination is distinct. - Fault with moderate offset but indistinct upward termination, allowing multiple interpretations for the event horizon during which this fault slipped. Nonetheless, there is reason to prefer association of this indicator with one of these event horizons over the others. - Minor or gradual thickness changes across fault that could simply reflect depositional gradients rather than filling of earthquake produced depression. - Folding amplitude small, and thickness change above horizon of folding is moderate, but stratigraphic location of the lowest unfolded layers is indistinct enough to allow for multiple interpretations for the event horizon during which this folding occurred. Nonetheless, there is reason to prefer one of these event horizons over the others. - Possible fissure which could alternatively be interpreted shear of a massive layer disrupted by multiple fault strands.
2	- Fault with moderate offset (≥ 5 cm), and indistinct upward termination, but the indicator can still be clearly associated with one event horizon. - Folding amplitude small, and thickness change above horizon of folding is moderate.
3	- Fault tip with distinct upward termination, moderate offset (≥ 5 cm). - Folding and thickness changes in layers above folding horizon that are substantial (~20 cm), but folding horizon has no clearly causative fault and (or) the horizon of folding difficult to discern. - Possible fissure for which the fill material does not clearly postdate the inferred event horizon, and both walls of the fissure are faults that have re-ruptured in a younger event
4	- Fault tip associated with colluvial wedge or layer thickness changes that reflect modification or erosion of scarp. - Possible fissures for which the fill material does not clearly postdate the inferred event horizon, but a least one wall of the fissure is a fault with a distinct upward termination, which has not re-ruptured in a younger event. - Broad warping and large thickness changes in layer above folding horizon indicate rapid filling of depression, closely related to fault that moved to provide accommodation space.
5	- Fissures that are clearly filled with the material that postdates inferred event horizon. - Folding and growth strata in which it is clear that the topography was rapidly filled by a single sedimentation event and has a casual fault.

(modified from Scharer et al., 2017 to reflect depositional characteristics of 18th Avenue site).

In some cases, faults with up to 20 cm of vertical separation have terminated at different stratigraphic levels during the same prehistoric earthquake (Weldon et al., 2002). In other cases, faults with displacement of only a few millimeters or less have ruptured to the ground surface (e.g., McGill and Rubin, 1999). Our selection of 5 cm to define “moderate” offset falls between these values. (2) In cases where the upward termination of a fault is not distinct, we assign a quality ranking of 0 when there is more than one identified earthquake horizon that could reasonably be projected between the highest stratigraphic level to which the fault can be traced and the lowest stratigraphic level that is clearly undisturbed by the fault in question. However, if the upward termination is not distinct, but there is an unfaulted unit that lies below the next higher earthquake horizon, then we assign a quality ranking of 1, for minor offset and 2 for moderate offset, because this is clearly a distinct event from the next younger event, even if the precise location of the earthquake horizon cannot be determined. (3) Scharer et al., (2017) made a distinction between folding and thickness changes that are “small” versus “substantial” with the latter being viewed as more likely to have resulted from deformation of the ground surface thus meriting a higher quality ranking. We considered thickness changes of 20 cm or more to be “substantial”, thus meriting a ranking for 3 (if a causative fault is not clearly identifiable) or 4 (if a causative fault is identifiable). Our selection of 20 cm reflects our judgement that folding and thickness changes smaller than this have a greater potential to result from non-tectonic causes.

Stratigraphic Correlation Rankings

Uncertainty in stratigraphic correlations led to difficulty determining whether some of the event indicators were at the same stratigraphic level or not. Because of the great width of the trench, only four distinctive layers could be correlated between the east and west walls. Even along the same wall of the trench, lateral facies changes, channel scour and some areas of poor stratigraphy, made it difficult to trace some of the stratigraphic units over long distances even in the absence of faults. Many strata could be clearly correlated across faults with minor offset, but stratigraphic correlation was more difficult across a few of the faults with larger amounts of offset.

To address the uncertainty in stratigraphic correlation of event indicators, we created a stratigraphic correlation ranking table (Table 4). This correlation ranking table requires that a type locale be defined for each individual event. We selected the type locale from among the best ranked event indicators for that specific event and with the additional criterion that it should be in a location in which it was possible to correlate layers between the type locale and the other event indicators. The event horizon for each other individual indicator is correlated along the trench wall (i.e., within a particular stratigraphic package) to the type section. Based on the continuity of the package, we assign it a stratigraphic correlation rating (1-5). A rating of five means an event indicator is easily followed all the way to the type section confirming it is at the same stratigraphic level as the event horizon at the type section. A rating of one means

that the correlation is uncertain enough to create ambiguity as to with which event this indicator should be associated. This may result from pinch out of marker beds, mismatch or changes in character of units across faults, benches and/or bioturbated zones.

Table 4. Description of Stratigraphic Correlation Rankings

Quality	Description
1	Stratigraphic correlation of one or more event horizons is uncertain enough to create **ambiguity** as to with which event this indicator should be associated.
2	The stratigraphic level of the indicator cannot be physically traced all the way to the type locale, because it crosses more than one fault, bench, or area of poor stratigraphy, leading to a **relatively high level of uncertainty**, including the possibility that the indicator could correlate with an event other than the proposed event.
3	The stratigraphic level of the indicator cannot physically traced all the way to the type locale, because it crosses a fault, a bench, or an area of poor stratigraphy. The correlation of strata is **somewhat uncertain**, but correlation with the proposed event is much more likely than correlation with any other recognized event. This rating may be applied to an indicator on the opposite wall from type locale for the event, as long as it is not far above or below one of the three layers that have been correlated between the walls (units E/W 290, E/W 610, or E/W 850).
4	The stratigraphic level of the indicator cannot be physically traced all the way to the type locale, because it crosses a fault a bench or an area of poor stratigraphy, but the correlation of strata is **fairly certain**. This rating may also be applied to an indicator on the opposite wall from type locale for this event, as long as it is not far above or below one of the three layers that have been correlated between the walls (units E/W 290, E/W 610, or E/W 850)
5	The stratigraphic level of the indicator can be **physically traced** all the way to the type locale, with no uncertainty in correlation of strata across any faults located between the indicator and type locale. This can only be true for indicators that are on the same wall as the type locale for event.

Characterizing the Likelihood of Each Event

We qualify the likelihood of a paleoearthquake at each stratigraphic horizon based on the quality and the number of individual event indicators in each paleoearthquake horizon. Following the example of Scharer et al. (2017), we use the terms *probable*, *likely* and *very likely* to denote horizons with increasing probability of representing a paleoearthquake horizon. Also, like Scharer et al. (2017), we aim use the label *probable* when the number and quality of event indicators suggest at least a 50% likelihood of a surface-rupturing event at that horizon. At this site, we consider events that have three or more indicators with at least one having a quality rating of 2 or higher to be probable earthquakes. Those with one or two indicators with quality rankings of 3 or higher are considered *likely*, or *very likely*, respectively (Table 5). Horizons with isolated, weak evidence that do not meet these criteria are not given an event number.

Table 5: Criteria for Characterizing the Likelihood of Events.

Probable	Three or more individual event indicators, with at least one of 2 or higher; None higher than a quality rank 2.
Likely	At least one event indictor with a rank of 3 or higher. Must have 3-5 individual event indicators with at least a rank of 1.
Very Likely	Two or more event indicators with a rank of 3 or higher.

CHAPTER FOUR

RESULTS

The orthorectified, georeferenced and annotated photomosaics for the west and east walls of the trench are shown in Plate 1. A cross-section line-drawing of the contacts and faults extracted from plate 1 is shown in Figure 3. Within Plate 1, strata that could be traced were assigned unit numbers, with unit numbers increasing with stratigraphic depth.

Because of the great width of the trench (22-m at the top), only a few units could be easily correlated between the west and east walls. The uppermost of these correlable units is unit 290, which is a 30-cm-thick silt layer with a distinct thin, brown clay at the base. This unit contained an abundance of charcoal pieces, more so than any other unit within unit within the trench. The next correlable unit is unit 610. On the east wall, this unit is distinguished by the presence of a number of large boulders (~ 0.5 m diameter) within an 0.5- to 1-m thick unit of coarse sand with pebbles and granules. On the west wall, this unit is sandier and the boulders are smaller (~ 0.25 m), but this is still the coarsest unit on the west wall, and is at a similar depth below the surface. Immediately below unit 610 is unit 620, which is composed of course sand, pebbles and small boulders (~0.25 m diameter) on the west wall and pebbly gravel on the east wall. The lowermost correlable unit is unit 850. This is a muddy sand and gravel unit

with a sharp contact at its top. The unit is brownish in color compared to overlying units that are more gray in color.

These four correlable units were used to anchor the stratigraphic numbering of units between the trench walls. Because no other units could be readily correlated between the two walls of the trench, all units on the west wall have “W” prefix before the unit number, and those on the east wall have an “E” prefix. Unit numbers between 0-99 were assigned to strata above the event 1 horizon; numbers between 100 – 199 were assigned to strata between the event 1 and event 2 horizons, and so on. Except for units 290, 610, 620 and 850, units that have the same number but a different prefix (E vs. W) should not be interpreted as correlating, nor should units with a lower number on one wall necessarily be assumed to be younger than a unit with a higher number on the opposite wall. Uncertainties in correlation of the event horizons were addressed through the correlation ranking system described above (Table 4).

Some unit labels also include a suffix letter after the unit number. In regions where a layer could be traced or correlated with certainty the suffix letter is the same. In cases where there was some uncertainty in the correlation of the layer across a fault, bench or region of poor stratigraphy, a different suffix letter was used on the two sides of the cause of the uncertainty. For example, unit W110A is a very fine sand layer that crosses a fault at 8 m on the west wall, tier 2 (Plate 1 and Figure 5). The figures show a possible correlation of unit W110

across this fault, but because the correlation is uncertain (e.g., not confirmed by other layers offset with a similar sense and amount), we call this unit W110B on the opposite side of this fault, indicating a proposed but uncertain correlation. Similarly, at 12 m on the west wall, tier 2, we make a proposed, but uncertain correlation of this unit across an area of poor stratigraphy, so the unit is labeled W110C on the other side of this area.

Earthquake Horizons

Appendix B lists and describes all of the indicators for each event at the 18th Avenue site. The data set of event indicators is summarized in Figure 4. This figure illustrates the number of indicators for each event, as well as their quality and stratigraphic correlation rankings. Applying Table 5, we have one *very likely* event (BF-1), four *likely* events and three *probable* events.

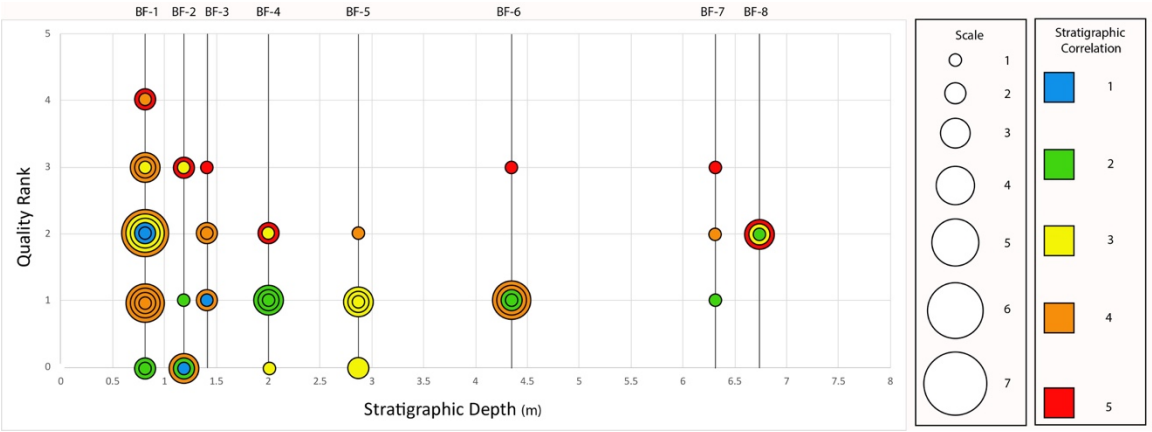

Figure 4. *Summary of Event Indicators. Eight paleoearthquake horizons were identified in the 18th Avenue trench on the Banning fault. Events are arranged according to stratigraphic depth on the horizontal axis. Vertical axis indicates quality ranking of each indicator, with higher numbers indicating better quality. The diameter of the symbol is scaled by the number of indicators in each rank. For example, earthquake horizon BF-1 has 5 individual event indicators with a rank of 2, producing a symbol diameter of 5. Color of the symbols represents the stratigraphic correlation ranking of each event indicator. Indicators with a warmer color can be correlated to the type section of the event with greater certainty.*

BF-1. *Very Likely.* The most recent paleoearthquake at the Banning Strand paleoseismic site has sixteen event indicators. There are three pieces of evidence with a ranking of 3 and two with a ranking of 4 (Plate 1, Appendix B), which all involve sharp upward termination of faults with more than 5 cm of vertical separation and/or stratigraphic units that thin and pinch out against a scarp or folding horizon. An event indicator with a rank 3 is shown in Figure 5. Two of these five strong pieces of evidence were on the west wall, and three were on the east wall. Within each wall, the stratigraphic horizon containing the strongest evidence for event 1 could be traced with moderate to high certainty along the length of the trench wall. Although it was impossible to correlate individual layers in this stratigraphic range between the east and west walls of

the trench, the sediments were generally similar on both walls (discontinuous 2- to 10-cm-thick layers of coarse sand with granules, fine sand, and silt). We therefore make the assumption that the paleoearthquake closest to the present-day ground surface must be the same on both walls. There were also eleven lower-rated indicators, which were primarily faults that terminated upward but had either very small amounts of vertical separation, or it was very difficult to locate the exact position of termination. All these event indicators were at the same approximate stratigraphic position as the stronger lines of evidence for event 1.

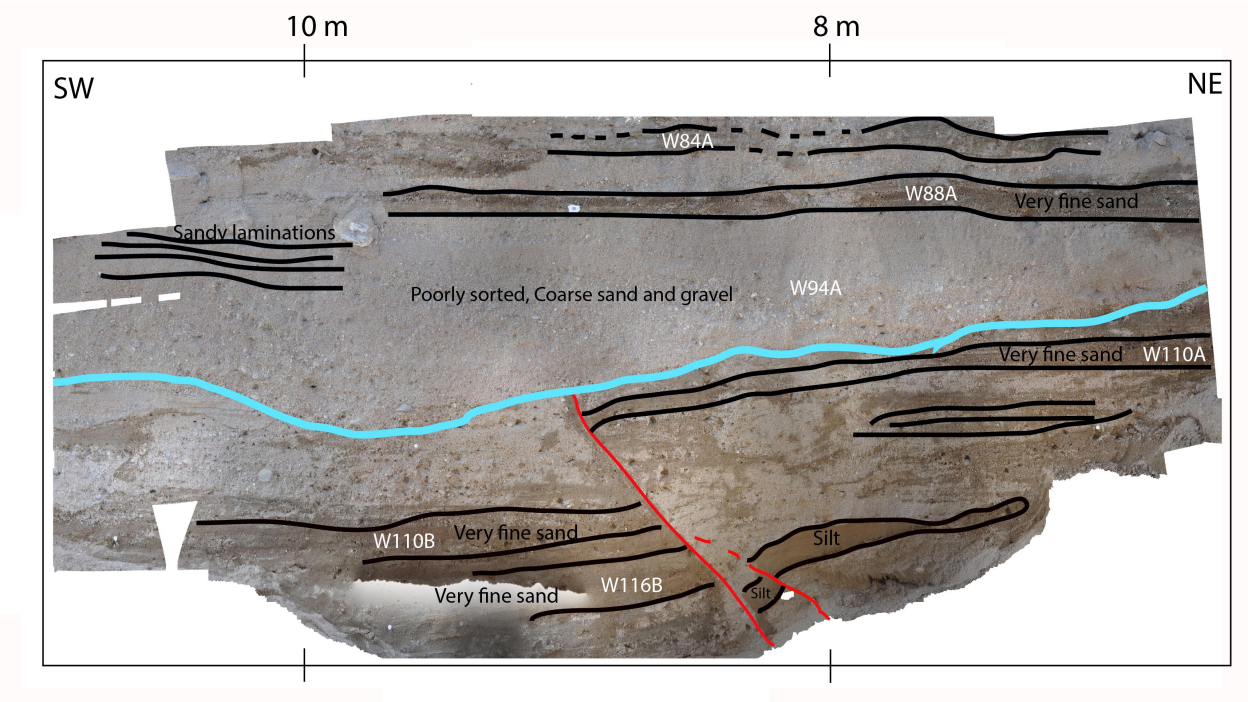

Figure 5. *Event 1 Evidence. Indicator for event BF-1 at 8-10 m on Tier 2 of the west wall. A fault terminates sharply at the base of a channel scour (colored light blue). This fault displays at least moderate offset due to one of the following reasons: 1) There is a very fine sand layer that is visible on both sides of the fault and is labeled as W110A and W110B. If this layer is in fact the same layer, then there is at least 40 cm of vertical separation or 2) If layer W110A is not the same as layer W110B, then correlating layers across the fault is difficult and suggests a large amount of lateral offset.*

BF-2. *Likely.* There are six indicators for this event including two with quality rank 3, one rank 1 and three rank 0. The type locale for this event has a quality ranking of 3 and is located on the west wall tier 1 at 28 m (Figure 6). Layer W220E is vertically separated about 40 cm across a zone of 4 faults. Layer W170E is on top of a scour surface that appears to cap the faults, although earlier logging interpreted this layer as offset (correlating with W208E or W218E). Regardless of which interpretation is preferred, the event horizon would only shift slightly, and the age estimate for the event would not change since layer W108E thins and pinches out over the scarp which definitely caps event 2.

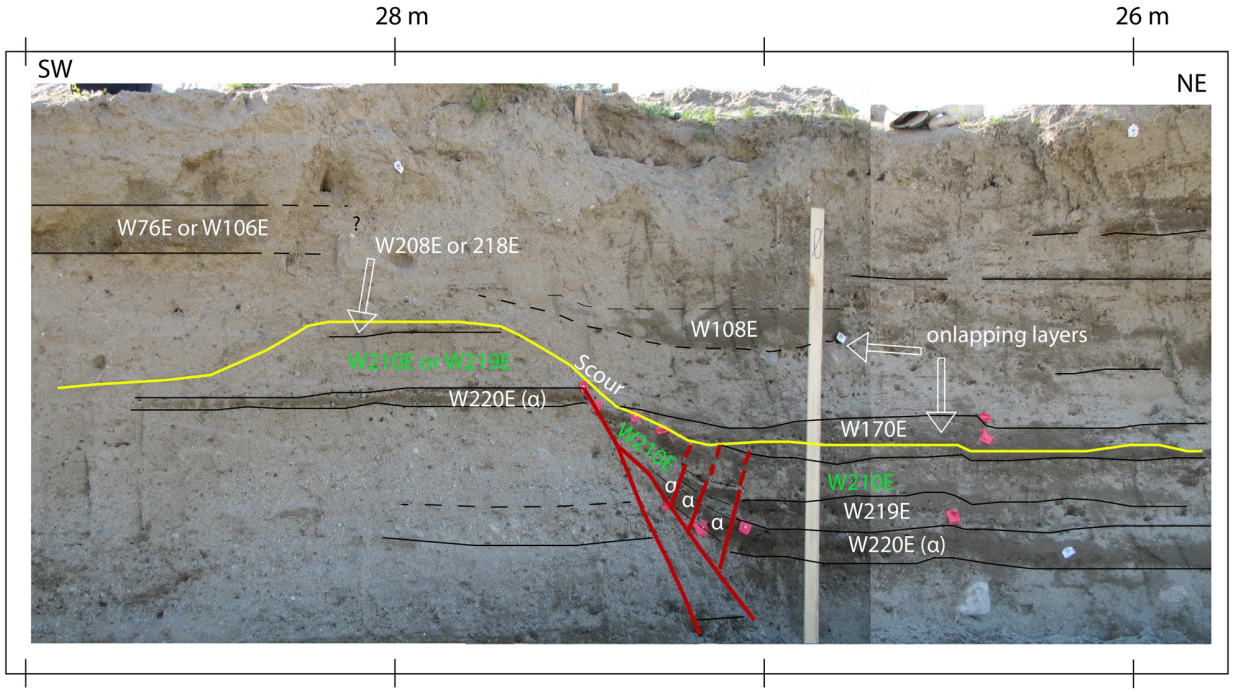

Figure 6. *Event 2 Evidence. Type locale for Event BF-2 at 26-28 m on Tier 1 of the West Wall. A series of faults terminate upward at the base of the yellow contact (Event 2 horizon), and the feature has a quality rank of 3. Nature of yellow contact indicates it scoured the ground surface after deposition of W210E, followed by onlap of W170E and younger.*

Another indicator for Event 2 is found on the East wall in Tier 2 at about 20 m, where a fault terminates upward at the base of a scoured channel (Figure 7). This fault has moderate vertical separation (12 cm) and layer E290 has been clearly offset. The fault can be traced to the base of a scour below which layer E210 is truncated by the fault. Layer E210 cannot be seen on the other side of the fault suggesting at least moderate lateral offset. This event indicator has a quality ranking of 3 but is on the opposite wall of the trench from the type locale, so we cannot say with certainty that these two indicators formed in the same earthquake. Nonetheless, they are both located stratigraphically below event 1 and above layer 290 (the base of which is the event 3 horizon), which we consider to be correlated with certainty between the two walls.

Additional supporting evidence for event 2 includes 3 event indicators that are found on the west wall (two quality rank 1's and one quality rank zero). On the west wall on tier 3 at 7 m there are distinct upward terminations of two faults with minor offset (rank 1). At 22 m there are two faults with indistinct upward termination and minor offset (Plate 1). Both of these faults terminate at a stratigraphic level that is lower than event 1, although the precise level of the event horizon is poorly constrained and the fault cannot be traced downward to tier 2. Lastly, there is an event indicator with quality rank 0, which is found on the east wall on tier 3 at 14 m. Here, there is a fault with moderate offset of layer E290 which stops at bench level in between tiers 2 and 3. Exact location of termination is unknown, but termination lies stratigraphically above the Event 3

horizon and below the Event 1 horizon suggesting it may have slipped during event 2.

BF-3. *Likely.* There are six event indicators for event 3, the ranks of which are 3, 2, 2, 1 and 1. The strongest evidence for event 3 (type locale) is the presence of a silt layer W290 on the west wall, centered within the main fault zone, near the north end of the trench, which thins and pinches out both to the south and to the north (Plate 1 and Figure 3). We interpret this silt layer to have been deposited within a graben that formed during event 3. Although the trench was not deep enough to reveal the faults that created this graben, it is clear on the west wall that a graben formed within the main fault zone (between 8-18 m) during event 2. Thus it is reasonable that a graben may also have formed here during event 3. We give this event indicator a quality rating of 3.

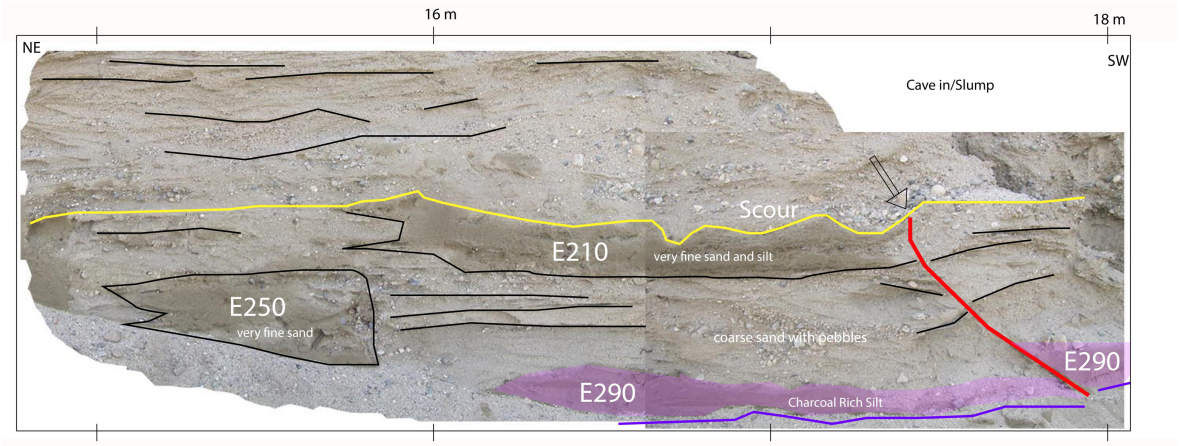

Figure 7*. Event 2 & 3 Evidence. Another indicator for Event BF-2 at 20 m of Tier 2 on the East Wall. The yellow line and purple line represent the event 2 and 3 respectively. Quality Rank: 3*

A distinctive feature of layer W290 is that this silt layer is richer in charcoal than any other silt layer within the trench. A similar charcoal-rich silt layer is also observed on east wall at a similar stratigraphic level and we correlate it with layer W290. On the east wall, layer E290 can be seen as far south as meter 20. Farther south, layer E290B was considered as a possible southward continuation of layer E290, but layer E290B is coarser and more poorly sorted than E290. We suspect that layer E290 may thin and pinch out in the vicinity of meter 20, but this is obscured by the incision of the trench wall by a small channel that formed after the trench was excavated. Because of the uncertainty as to whether layer E290 pinches out near meter 20 or continues indefinitely southward as layer E290B, we assign a quality rating of 1 for layer E290 as an event indicator.

Three other event indicators are all located on the east wall. First, in tier 3 at 18 and 19 m there are two faults with significant lateral offset (indicated by difficulty in correlating layers across the faults) that are visible to the top of tier 3 but not visible in tier 2 (Figure 8). Layer E290 lies at the base of tier 2, and is unfaulted over the fault at 19 m, so this fault probably ruptured during event 3 and we give this event indicator a quality ranking of 2. The event indicator at 18 m has a quality ranking of 2 because layer E290 lies at the bench level and is not exposed over this fault at the base of tier 2. Lastly, on tier 2 at 27 m there is a fault with minor displacement that is capped by layer E290B, which is at approximate stratigraphic level of layer E290 (and event 3). We give this

indicator a quality ranking of 1 because the fault only has minor displacement.

The stratigraphic correlation ranking for this indicator is 1 (see Appendix B).

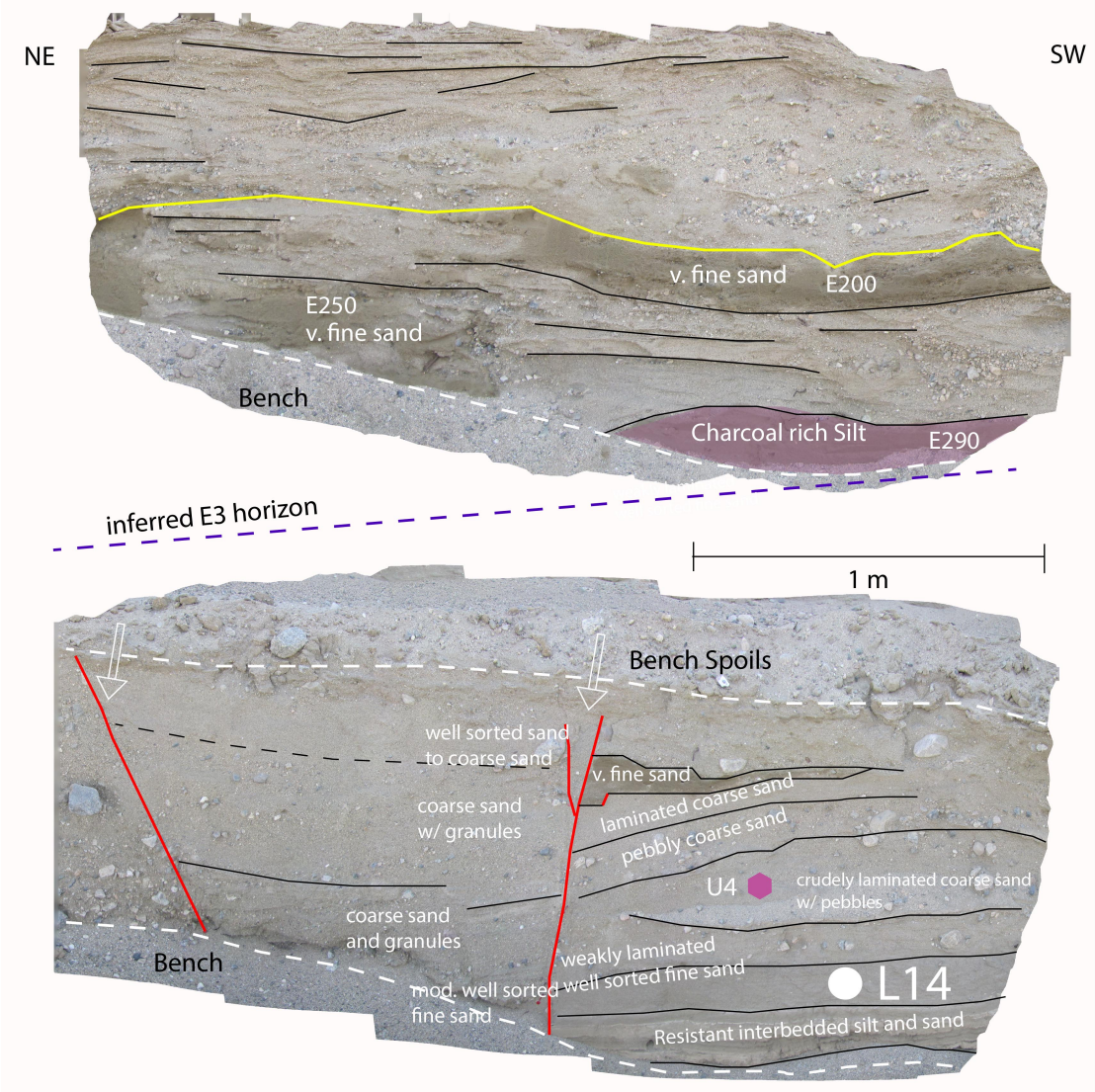

Figure 8. *Event 3 Evidence. Indicator for event BF-3 at 18-20 m on the East Wall inTier 2 (top) and Tier 3 (bottom). Both faults(left and center) terminate at the bench level between Tiers 2 and 3. Layer E290 can be seen at the base of Tier 2 and appears to be unfaulted, suggesting that the BF-3 horizon lies at the bench level. Dashed purple line between the two tiers marks the projection of the event 3 horizon where these two faults could potentially terminate. There is no evidence of any faulting seen on tier 2 in this vicinity. Mismatch of stratigraphy acros the fault on right supports lateral slip on this fault. Yellow line is the event 2 horizon.*

BF-4. *Probable.* There are six event indicators for Event 4 including two with rank 2, two with rank 1 and two with rank 0. The strongest evidence can be found on the west wall tier 1 at 32 m (type locale; Figure 9), where a fault has produced moderate vertical seperation of layer W405. This fault is capped by a scour horizon(spray painted green in Figure 9), which forms the base of a sandy channel that is unfaulted. The quality ranking is 2 because it is not clear whether the sharp scour contact is present continuously across the fault zone.

On the west wall on tier 2 at 23 m there is a fault with about 6 cm of vertical seperation (moderate offset) that is capped by layer W390, which appears to be unfaulted (Plate 1). The contact at the base of W390 is sharp directly above the fault, but lacks clear continuity on both sides of the fault, so we assign a quality rating of 2, instead of 3. The two event indicators just described are both on the west wall, but are separated by about 9 meters laterally and by a bench. Our correlation of stratigraphic units suggests that these two indicators are at approximately the same stratigraphic level. We assign a stratigraphic correlation rating of 3.

Also on the west wall on tier 3 at 22 m there is a fault with moderate offset of layer W555C. The fault could be capped by layer W470C, near the top of tier 3, or it could continue onto the base of tier 2, and be capped by W390C. In the latter interpretation, this fault would have slipped in event 4. In the former interpretation, this fault would have slipped in an earthquake between events 4

and 5. Due to the significant uncertainty in the location of the upward termination of the fault we assign it a quality ranking of 0.

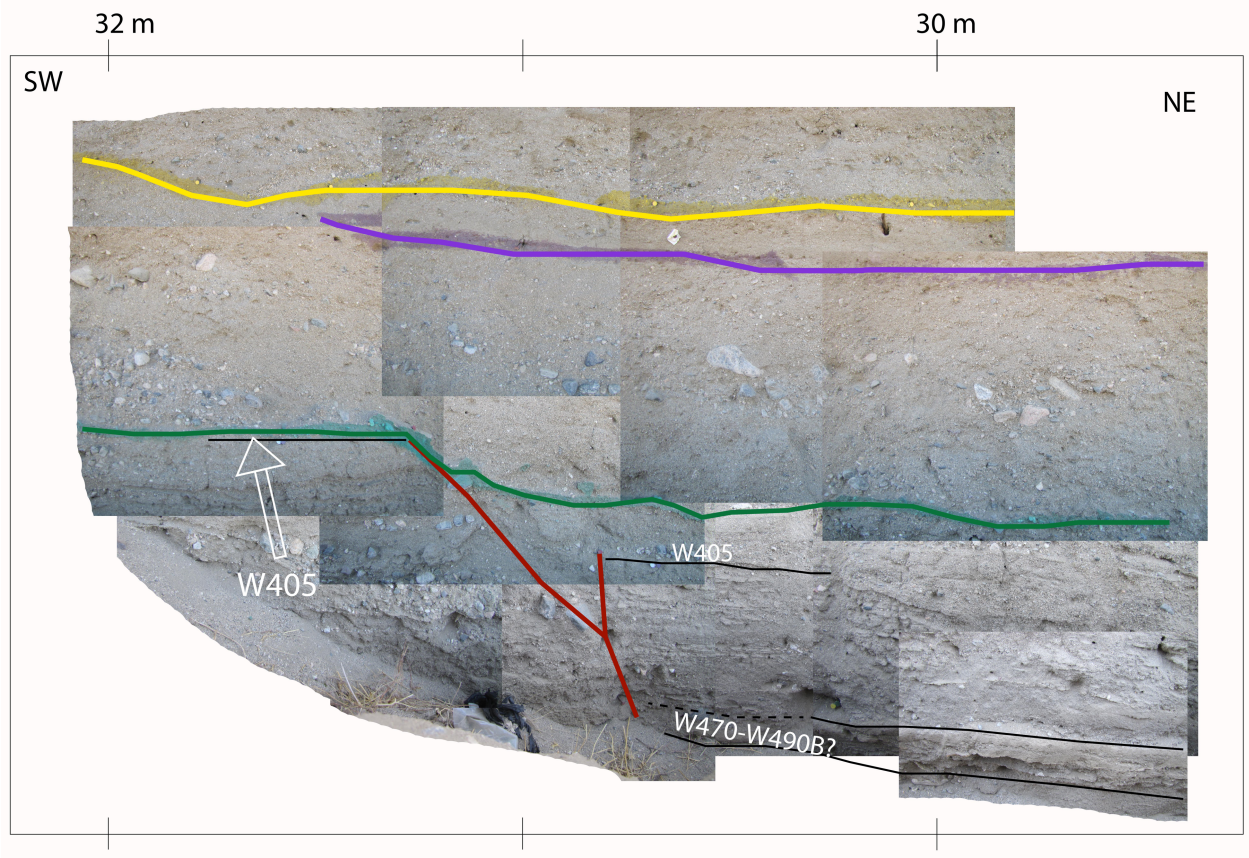

Figure 9. *Event 4 Evidence. Type locale for Event 4, at 30-32 m on Tier 1 of the West Wall. Lower part of figure includes photos from a hand-dug, deeper extension of Tier 1 that are not included in Plate 1. Green line spray painted on trench wall highlights the event horizon. A fault vertically separates layer W405 and is capped by a scour (green horizon) that forms the base of a sandy channel. The yellow and purple lines represent earthquake horizons 2 and 3, respectively.*

On the east wall on tier 2 at 32 m and 36 m, there are two faults that terminate upward with a minor vertical seperation (quality ranking 1). We cannot be certain that these faults slipped in the same event as event 4 on the west wall, but this would be the simplest interpretation and is compatible with the relative

stratigraphic position of this feature. Lastly, on tier 3 of the East wall at 24 m there is a fault with minor offset originally mapped as capped by unit E480 but which may extend upward and correlate with a fault in tier 2 which could potentially be event 3 and or possibly even event 4. Because of the uncertainty as to which event produced this indicator, it has a quality ranking of 1.

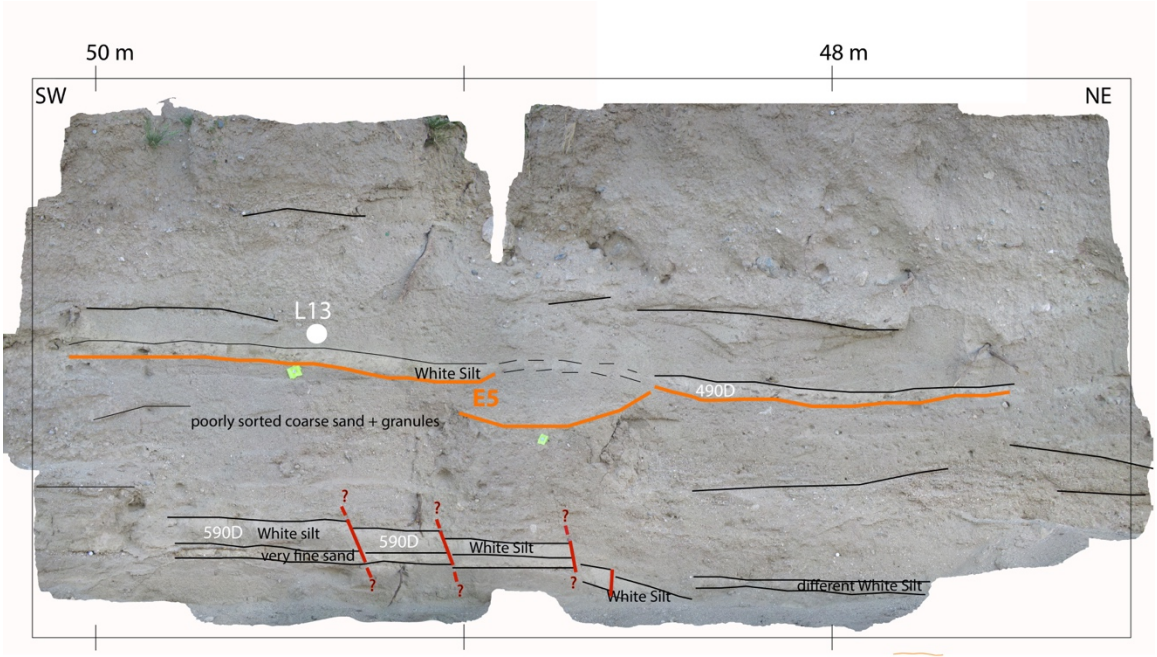

Figure 10. *Event 5 Evidence. Type locale for Event 5, at 48-50 m on Tier 1 of the West Wall.*

BF-5. *Probable.* There are 6 indicators for this event, including one rank 3, three rank 1s and two rank 0s. The best evidence and type locale can be found at 50 m on tier 1 of the west wall, where we observe 4 faults with minor vertical seperation of layer W590D that are all capped by the unfaulted layer W490D (Figure 10). Total vertical seperation across the zone is ~10 cm. Therefore, we

consider this moderate offset. The faults may terminate at or up to 20 cm below layer W490D. The 20-cm interval within which the earthquake horizon lies is bracketed by C-14 samples A18 and A24, as well as by luminescence samples L13 and L07; there are no dated samples from within this 20-cm interval. Therefore we consider this a distinct upward termination and assign these faults a quality rating of 3.

On the east wall, tier 3 at 26 m, three faults with minor offset downdrop debris flow layer E520 into a small graben that is capped by the unfaulted muddy silt layer E490 (Figure 10). We give each of these faults a quality ranking of 1. On the East wall at 23 m, we also observe a fracture in layer E520 that is weathering out and may connect downard to a fault (quality rank 0) (Figure 11). These indicators from the east wall are all clearly capped by the same horizon (E490). Also on the east wall, tier 2 at 32 m, there is a fault splay with unknown but likely very minor offset that is capped by layer E440. We assign a quality ranking of 0. Because E490 pinches out before reaching this location, E440 likley represents the first sediment deposited after event 5, and this fault splay likely slipped in event 5. Correlation of the evidence for event 5 between the east and west walls is uncertain, but represents the simplest interpretation.

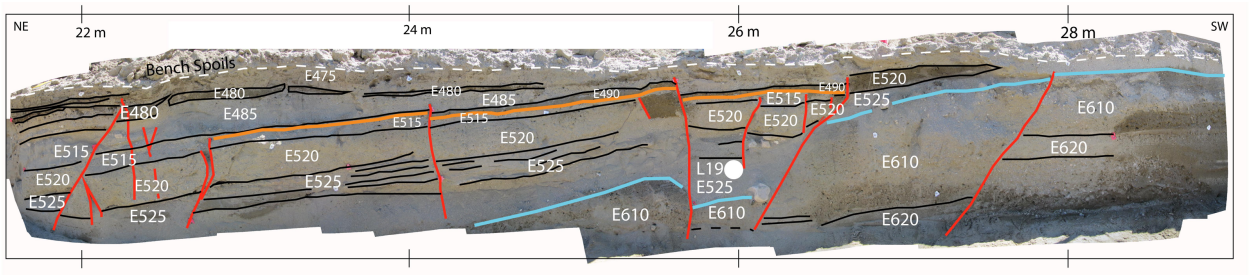

Figure 11. *Event 5 & 6 Evidence. Indicators for Events 5 and 6 at 21-27 m on Tier 3 of the East Wall. Several minor faults slipped in event 5 and are capped by an unfaulted layer E490. Layers E520 and E525 thin southward (right), suggesting they were deposited within a depression that formed during event 6.*

BF-6. *Likely.* There are five indicators for Event 6. There is one event indicator with a rank of 3, and four additonal event indicators with a rank of 1. The type locale is locaed on the east wall, tier 3 between 22 and 27 m. Here layers E520 and E525 thin from 60 cm of layer thickness at 23 m down to 20 cm at 26 m (Figure 11). We interpret that these layers were part of a post-earthquake deposition sequence that filled a closed depression that was formed during event 6, similar to the character of the basin-formation in more recent events. The large and rapid changes in unit thickness indicate filling of a depression and a quality ranking of 3. The earthquake horizon is interpreted to be at the top of layer E610, which is a thick, bouldery debris flow that does not have any readily noticeable thickness change across this region.

On the west wall, unit W610 consists of boulders within moderately well sorted course sand. We interpret this layer to be the westward continuation of debris flow deposit E610. At 23 m on tier 4 of the west wall, two faults produce minor vertical seperation within layer W610, and are capped by unfaulted layer W590 (Plate 1). We interpret these as indicators of event 6, with quality ranking

1. Farther south on the west wall, we tentatively correlate the thick clay layer W590 with silt layer W590B, W590C and W590D, which is the most laterally continuous silt layer to the south. At 38 and 39 m on tier 2 of the west wall, we observe two faults that have produced minor vertical seperation (~2 cm) of layer W604C and are capped by unfaulted layer W590C. If our correlation of layer W590 with W590C is correct, then these two faults provide additional indicators (quality rank 1) for event 6. However, it is also possible that layer W590 at 23 m correlates with layer W604C (at 36-50 m). If this alternate correlation is correct, then the two minor faults at 38 and 39 m would be indicators for an event between events 5 and 6.

BF-7. *Likely.* There are are three event indicators for event 7, one with rank 3, one with rank 2 and one with rank 1. The strongest evidence can be seen at the type locale on the east wall, tier 4 at 32 m. Here we observe an 80 cm thick package of very fine sand, silt and clay (E660-E690) that thins to 10-15 cm (E690) across a fault and then pinches out to the south (Figure 12). We gave this indicator a quality rank of 3 due to the substantial thickness change observed here. The causitive fault (at 32 m) has re-ruptured in younger earthquake.

The quality rank 2 indicator can be seen on the east wall, tier 3 at 36m (Figure 12). Here, we observe a fault with 5 cm of vertical seperation in the upper part of tier 4 (pebble layer E710), which is capped by an unfaulted fine sand layer (E690) at the base of tier 3. Because the fault and the capping layer are not

visible on the same tier this event indicator was given a quality ranking of 2 instead of 3. Correlation of units between 32-36 m on the east wall is clear enough that we are confident that these two indicators represent the earthquake horizon. The indicator at 36 m has thus been assigned a stratigraphic correlation ranking of 4 with respect to the type locale at 32 m.

The rank 1 indicator can be seen on the west wall, tier 4 at 28 m, where layer W690 thins to the south and pinches out. The causative fault is likely the fault at 28 m. Although we observe moderate thickness change, which suggests filling of a closed depression, layer W690 is only exposed over a short distance (about 2 m) so the full extent of the closed depression is not visible. Therefore we assign a quality ranking of 1. It is not clear whether layer W690 is the same as layer E690 on the opposite wall of the trench, but it is clear that on both the east and west walls, there is evidence for two events (events 7 and 8) below layer 610 and above layer 850, both of which can be correletated between the two walls of the trench with a relatively high degree of confidence.

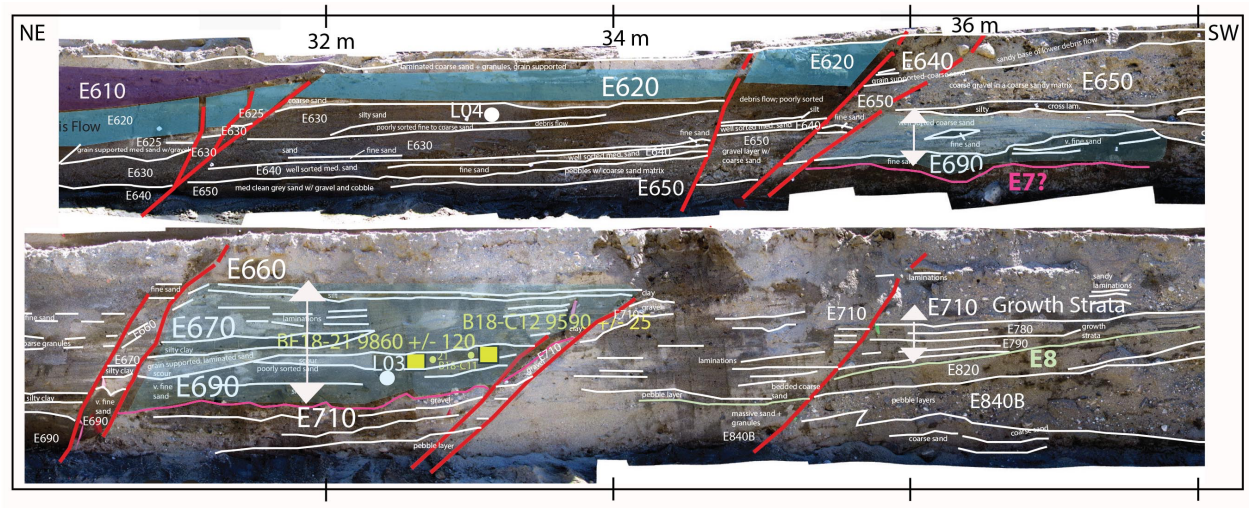

Figure 12: *Event 7 & 8 Evidence.Type locale for Event 7 at 30 m on Tier 4 of the east wall. Layers E660 – E690 can be seen thinning and pinching out as they extend to the south (Highlighted by light blue). An indicator for Event 8 at 32 on Tier 4 of the east wall. Layers E780-E790 thin to the south, filling a depression formed when layer E820 was tilted during Event 8.*

BF-8. *Probable.* There are three event indicators (all rank 2) for the oldest event horizon observed at this plaeoseismic trench site. Two event indicators with a quality rank of 2 are located on the west wall, tier 4 at 32 and 36 m (type locale). At the 32 meter mark there is a fault with moderate vertical seperation (22 cm) of layer W815-W815B which is then capped by a layer of fine sand (layer W790) (Plate 1). The base of layer W790 is sharp directly above the fault, but lacks clear continuity to the north, therefore we assign this a quality rating of 2, rather than 3. At the 36 meter location (type locale) we observed a fine sand layer (W790C) that thins towards the south and pinches out against a fault at 32 m. We infer that layer W790 filled a depression that formed during event 8. Only a small section of the thinning and pinching layer W790 is visible just below bench level. Therefore we assign a quality ranking of 2, rather than 3. We tentativley

correlate layer W790 with W790B and W790C, which would imply that these two event indicators confirm the same event horizon. However, there is some uncertainty in this correlation. In addition, it is not clear whether layer W790 is the same as layer E790 on the opposite wall of the trench. Nonetheless, it is clear that on both the east and west walls, there is evidence for two events (events 7 and 8) below layer 610 and above layer 850, and both of unit 610 and 850 can be correlated between the two walls of the trench with a relatively high degree of confidence.

At 36 m on tier 4 of the east wall, layers E780 and E790 thin and pinch out to the south, and we interpret them as growth strata. The causitive fault (at 34 m) has 40 cm of vertical seperation on layer E840B (below the growth strata) but only 5 cm of vertical seperation on layer E710 above the growth strata section. This suggests that 35 cm of vertical separation occurred on this fault during event 8, and an additonal 5 cm occurred during event 7. Observation of layers E780-E790 changing thickness, with a casautive fault with moderate to large offset leads us to give this event indicator a quality rank of 2.

CHAPTER FIVE

PALEOEARTHQUAKE AGES

Radiocarbon and Luminescence Dating

The depositional timing of layers is provided by 33 detrital charcoal samples dated with radiocarbon dating and 17 sediment samples dated using post-IR IRSL techniques (Tables 1 and 2). All dates are plotted in Figure 13 as a function of stratigraphic depth. Stratigraphic depths were measured at 24 m on the west wall down to layer W620, and then at meter 34 for layers older than W620. This type section was selected because it is within a broad fault-bounded block with coherent stratigraphy, yet it also is close to the area where layers are thickest. Samples from the east wall, as well as samples from the west wall that are from a different fault block than the type section are shown with vertical error bars that illustrate the uncertainties in the stratigraphic positions of these samples relative to the type section.

Many studies have shown that it is not uncommon for detrital charcoal samples to overestimate the age of the layer from which they were collected by an amount that depends on the length of time between when the wood within the sample stopped growing and when the sample was deposited in the location from which it was collected (*e.g.*, McGill et al., 2002; Fumal et al., 2002a). We therefore ignore any charcoal samples with dates that are older than other charcoal or luminescence samples from the same layer or from lower layers. We

are comfortable with this approach because we were careful in the field to avoid collecting any charcoal or luminescence samples from obvious filled burrows or potentially bioturbated zones, and we reviewed photographs of the sample locations to evaluate the potential for unrecognized bioturbation at each sample location.

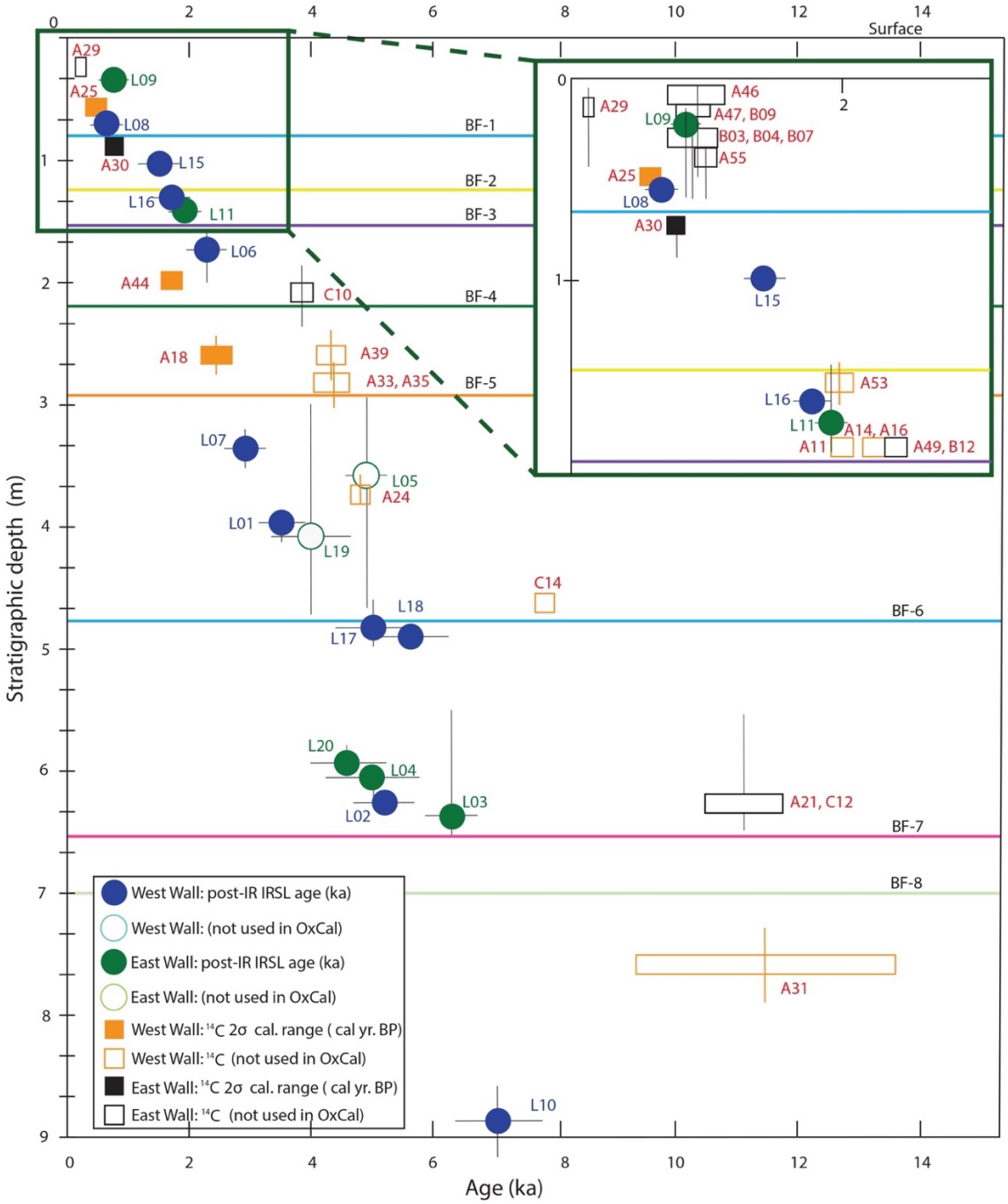

Figure 13. *Calibrated Radiocarbon and Post-IR IRSL Ages as a Function of Stratigraphic Depth. Stratigraphic depth was measured on the west wall at 24 m (for layers 20 - 620) and at 34 m (for layers 620 - 850). Vertical error bars show uncertainties in correlating sample locations from the east wall or from other fault blocks on the west wall with the type section. Solid symbols show ages that were included in our preferred OxCal model; open symbols show samples excluded from that model.*

In Figure 13, dated samples that are included in our preferred age model are plotted with filled symbols, and those that are excluded are plotted with open symbols. As can be seen, 29 out of 33 radiocarbon dates have been omitted from our preferred age model, which instead relies heavily on the IRSL ages to constrain the timing of past earthquakes. Omission of this many samples is justified because where we have multiple samples from the same depths (e.g., at 2 and 2.75 m stratigraphic depth) mean radiocarbon ages are separated by as much as 2000 years. Two IRSL samples from the east wall (L05 and L19) were also excluded from our preferred age model because of large uncertainties in their stratigraphic depth relative to the type section on the west wall. Using our preferred age model, the stratigraphic thickness of 9 meters that was exposed in the trench was deposited within the past 7600-6000 years, suggesting an average depositional rate of 0.11-0.15 cm/yr. The dated samples suggest a relatively constant sedimentation rate. The longest possible depositional hiatus is 1 - 1.5 k.y. between samples L01 and L17. Samples L17, L18, L20, L04 and L02 all have nearly same age, despite spanning about 1.5 m of stratigraphic depth. This is not surprising given that this depth range is dominated by the two thickest units in the trench, the boulder units 610 and 620, which may have been deposited very rapidly, potentially during the course of two storms.

Paleoearthquake Model Ages

We used the on-line software OxCal (Bronk Ramsey, 2009) to estimate the earthquake ages using the samples that define our preferred age model. For comparison, earthquake ages estimated using an alternate age model are reported in Appendix C. OxCal uses Bayesian statistics to model posterior ages for the paleoearthquakes based on all chronological constraints such as relative stratigraphic position. Dates from the same layer, or from layers that might correlate with each other were included in the same "phase". The results of the OxCal run on our preferred age model are shown in Figure 14 and Table 6.

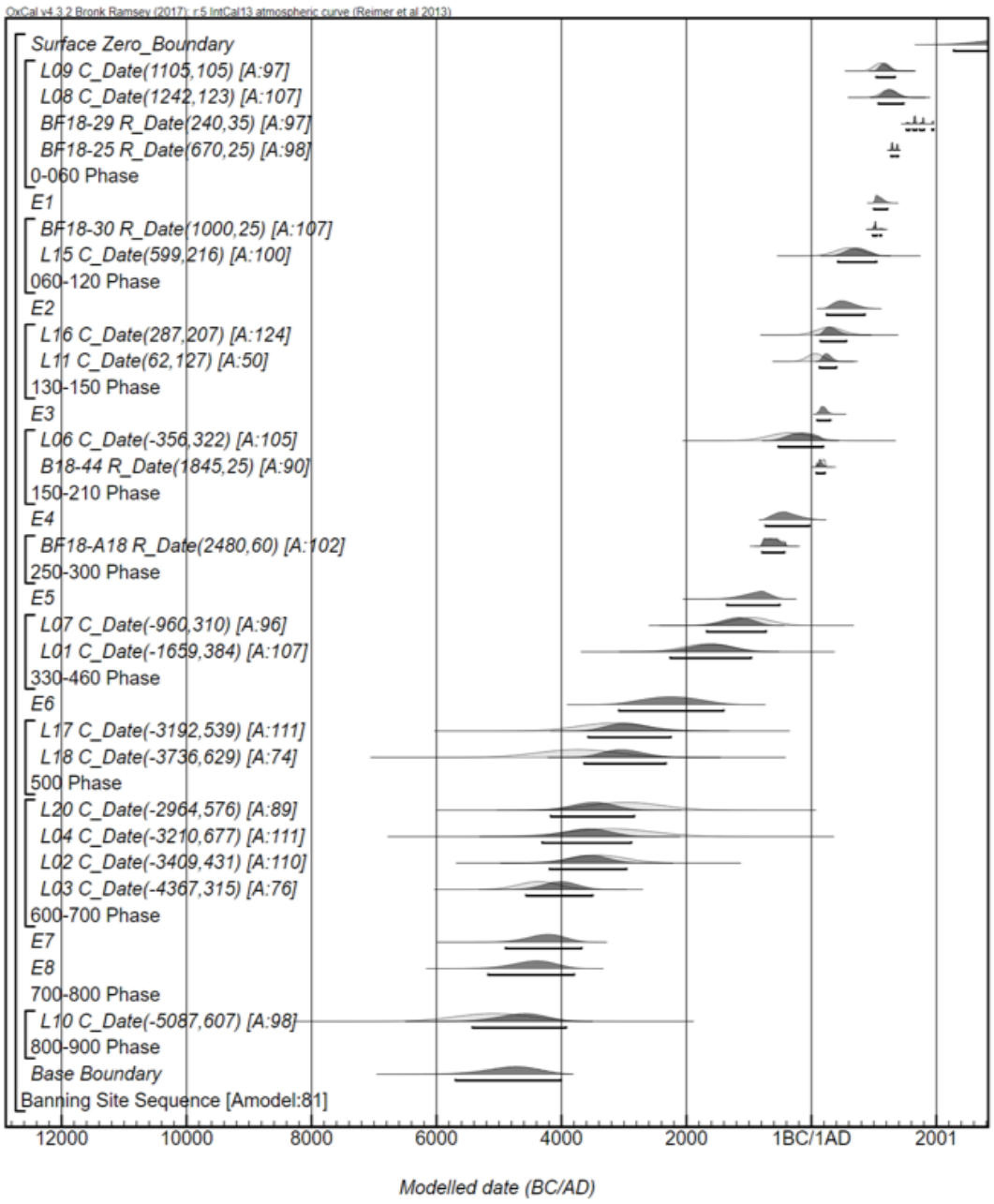

Figure 14*. Oxcal Model to Estimate Earthquake Ages. These ages are plotted as a function of stratigraphic position. Curves shaded light grade are the a priori probability density functions obtained for the ages of individual samples. Curves shaded in dark gray are the posterior probability density functions for each sample. In the Bayesian approach used within OxCal, the ages of samples above and below a given sample are used to reweight the probability density function for that sample so as to yield a set of ages that are stratigraphically consistent with each other as well as being consistent with the a priori (measured) ages of each sample.*

Table 6. Ages of Radiocarbon (R_Date) and Luminescence (C_Date) Samples and Paleoearthquakes.

		Unmodeled (BC/AD)		Modeled (BC/AD)		BP		
		from	to	from	to	from	to	Mean Age
Boundary Surface				2271	7022			
C_Date L09		895	1315	1041	1336	909	614	
C_Date L08		996	1488	1073	1476	877	474	
R_Date A29		1522	...	1521	1953	429	-3	
R_Date A25		1276	1390	1276	1390	674	560	
E1				1000	1217	950	733	818
R_Date A30		987	1149	984	1118	966	832	
C_Date L15		167	1030	424	1040	1526	910	
E2				248	855	1702	1095	1366
C_Date L16		-128	700	144	559	1806	1391	
C_Date L11		-193	315	129	399	1821	1551	
E3				93	303	1857	1647	1718
C_Date L06		-1000	286	-529	189	2479	1761	
R_Date A44		87	238	80	216	1870	1734	
E4				-735	-32	2685	1982	2333
R_Date A18		-777	-416	-789	-433	2739	2383	
E5				-1353	-508	3303	2458	2842
C_Date L07		-1582	-342	-1674	-727	3624	2677	
C_Date L01		-2427	-894	-2253	-967	4203	2917	
E6				-3086	-1402	5036	3352	4122
C_Date L17		-4270	-2118	-3566	-2251	5516	4201	
C_Date L18		-4993	-2482	-3629	-2332	5579	4282	
C_Date L20		-4116	-1816	-4171	-2838	6121	4788	
C_Date L04		-4564	-1860	-4303	-2883	6253	4833	
C_Date L02		-4271	-2550	-4185	-2962	6135	4912	
C_Date L03		-4999	-3739	-4556	-3491	6506	5441	
E7				-4885	-3663	6835	5613	6266
E8				-5167	-3782	7117	5732	6500
C_Date L10		-6301	-3877	-5423	-3910	7373	5860	
Boundary Base				-5687	-3994	7637	5944	

CHAPTER SIX

DISCUSSION

As shown in figure 4, the overall number of observations and quality rank of event indicators decreases with depth. There are several reasons why the evidence for older events is weaker than for the younger events. First, the older strata are only exposed within a small portion of the fault zone, so there is less opportunity to find event indicators associated with older events. Second, evidence for older events has been overprinted by younger earthquakes, making interpretation more difficult. Stratigraphic correlation of event indicators to their respective type locales was also a major challenge in this trench at all stratigraphic levels, but was compounded for older events due to increased difficulty in correlating layers across faults in which the cumulative lateral offset in multiple events was large.

Recurrence Interval

The earthquake record at the site includes up to five events in the upper three meters, which occurred in the past 2.4 - 3.3 ka (age range for event 5). On the other hand, only three events occurred in the lower 6 meters, during a 2.6 - 4.7 k.y. period between events 5 and event 8. We have no indication from the age model that any significant hiatuses occurred in the section (i.e., the sedimentation rate is reasonably linear). This suggests that either we are

missing events in the lower section, or the recurrence pattern at the 18th Avenue site is variable. We cannot rule out the possibility that the record of older earthquakes at this site is incomplete, because, as noted above, (1) the stratigraphic levels at which events 6-8 occurred are not exposed in the graben, which we interpret to be the main fault zone, and (2) ruptures in younger events may have obscured evidence for older ruptures on the same fault strands.

Using only the five most recent events, the maximum recurrence interval for the Banning strand is 640 years, based on four complete earthquake cycles between the youngest possible age for event 1 (730 cal BP) and the oldest possible age for event 5 (3300 cal BP). The minimum recurrence interval is 380 years, based on four complete earthquake cycles between the oldest possible age for event 1 (950 cal BP) and the youngest possible age for event 5 (2460 cal BP). The recurrence interval for the entire trench is 680 to 910 years, with the minimum recurrence interval being calculated based on seven complete earthquake cycles using the oldest possible page of event 1 (950 cal BP) and the youngest possible age for event 8 (5730 cal BP). The maximum recurrence interval is calculated using the youngest possible age for event 1 (730 cal BP) and the oldest possible age for event 8 (7120 cal BP).

Comparison to Other Paleoseismic Sites

The most recent 18th Ave event on the Banning strand of the San Andreas fault occurred between 950 – 730 cal BP. When comparing this to neighboring paleoseismic sites there are several important observations. 1) The MRE at the

18th Avenue site is much older than the MRE at three paleoseismic sites on the Coachella Strand which include: Coachella site (~280 cal BP; Philibosian et al., 2011), Indio site (~270 cal BP; Sieh and Williams, 1990), and Thousand Palms site (430-270 cal BP; Fumal et al., 2002a). 2) The MRE on the San Gorgonio Pass thrust occurred 750-630 cal BP (Wolff, 2018), slightly overlapping with the MRE on the Banning strand. 3) The MRE for the Garnet Hill fault is >600 BP, indicating that this fault may have ruptured with the MRE on the Banning fault, or its MRE may have been even older. 4) The penultimate event on the San Gorgonio Pass thrust (1220-1100 cal BP; Wolff et al., 2018) also overlaps with the penultimate event at the 18th Avenue site (1700-1100 cal BP). 5) The recurrence interval between the past five surface-rupturing earthquakes at the 18th Avenue site (390- 610 years) is longer than it is for the three sites on the Coachella strand (116-300 years; Philibosian, 2011, Sieh and Williams, 1990, Fumal, 2002a) and overlaps with the published recurrence interval at the San Gorgonio pass site (~450-1850 years; Wolff, 2018).

Implications for Slip per Earthquake

The Banning strand of the San Andreas fault has a slip rate of 2.3–6.2 mm/yr and accommodates about ~25-35% of the motion in the southern San Andreas fault zone (Gold et al., 2015). Using our age for the most recent event (950-730 cal BP) and the slip rate on the Banning Strand, we estimate the fault may be ready to produce slip of 1.7-5.9 m in the next earthquake (Table 7).

Using the average recurrence interval of 380-640 years between events 1-5 and the slip rate, we estimate that the average slip in these past five events was 0.8 – 3.9 m.

Table 7. Slip Implication Calculations.

	Min	Max
Slip Rate (mm/yr)	2.3	6.2
RI Range (years)	380	640
Avg. Slip per event (m)	0.87	3.97
MRE (Cal BP)	730	950
Accumulated Slip (m)	1.68	5.89

CHAPTER SEVEN

CONCLUSIONS

The 18th Avenue site provides the first paleoseismic record constructed on the Banning Strand of the SSAF and this record can now be compared to paleoseismic records on the neighboring strands that make up the complex network of faults in the southern section of the San Andreas Fault. The relatively high depositional rate and the structural setting of this site, a small pull-apart basin that has grown incrementally in earthquakes over the last 7,000 years, create a valuable paleoearthquake record. Eight horizons were identified as paleoearthquakes based on sedimentological responses to deformation and fault terminations at each horizon; BF-1 is considered *Very Likely;* BF-2, BF-3, BF-6, and BF-7 are considered *Likely;* BF-4, BF-5 and BF-8 are considered *Probable.* Dating constraints for earthquake horizons are best in the upper 5 earthquakes, as are the event quality so we focus on that part of the record. The most recent event occurred 950-730 cal BP and the average recurrence interval between Events 1-5 is 380-640 years, suggesting that fault may be overdue for a large, ground-rupturing earthquake. Based on a previously published slip rate, the next event may be expected to have at least 1.7-5.9 m of slip. The two most recent events on the Banning strand are similar in age to the most recent event on the San Gorgonio Pass thrust but are older than the most recent events on the Mission Creek strand of the SSAF. The average recurrence interval for Events

1-8 is 680-910 years, but it is possible that this overestimates the true recurrence interval because older events may have occurred without being recognized due the limited exposure of deeper strata within the fault zone and overprinting of older events by younger faulting.

APPENDIX A

DETAILS OF THE LUMINESCENCE DATING METHOD AND RESULTS

K-feldspar grains of 175–200 μm diameter were isolated from the sedimentary samples under dim amber LED light conditions. Subsamples were wet-sieved and separated by density with lithium metatungstate (ρ <2.565 g/cm^3; Rhodes, 2015). Luminescence measurements were carried out using a TL-DA-20 Risø automated reader equipped with a single-grain IR laser (830 nm, at 90% of 150 mW; Bøtter-Jensen et al., 2003) and a 90Sr/90Y beta source. Emissions were detected using a photomultiplier tube with the IRSL signal passing through a Schott BG3- BG39 filter combination. Samples were mounted on aluminum single-grain discs with 100 holes. The gamma dose-rate was measured in situ using a calibrated, portable NaI gamma spectrometer except for one sample (L11).

The U and Th concentrations were measured with inductively-coupled plasma mass spectrometry (ICP-MS), and the K concentration was measured using inductively-coupled plasma optical emission spectrometry (ICP-OES). These values were used to calculate the total beta dose rate contribution using the conversion factors of Liritzis et al. (2013). A value of 12.5 ± 0.12 wt. % K content was used in calculating the internal dose-rate (Huntley and Baril, 1997). The cosmic ray contribution was calculated from the burial depth and the latitude and altitude of the samples (Prescott and
Hutton, 1994; Table 2). We determined the water content for each sample from their weights before and after drying. The total geologic dose rate was calculated using the DRAC online calculator (v.1.2; Durcan et al., 2015).

A post-IR IRSL protocol (Buylaert et al., 2009) was used to measure the equivalent dose (De) values for individual grains. Each grain was stimulated first at 50° C for 3 s, and then at 225° C for 3 s to measure the more time-stable post-IR IRSL signal. A preheat of 250° C for 60 s was used before natural and regenerative measurements, and a hot bleach with IR diodes at 290° C for 40 s was added to the end of each SAR cycle (Wintle and Murray, 2006).

Samples were given a beta dose of 22 Gy, preheated at 250° C for 60 s and left at room temperature for timescales ranging from about 300 s to 7 days to test for the presence of athermal fading (Huntley and Lamothe, 2001). We performed these measurements on eight (L02, L04, L05, L10, L11, L18, L19, and L20) of the seventeen samples and four of those samples (L02, L10, L11, and L19) showed slight fading.

We are currently conducting more rigorous fading measurements on 13 samples, including the four samples that showed fading (Table 2). Fading corrected ages, therefore, will be made available soon. We used strict rejection criteria: 10% recycling ratio and maximum test dose error, and maximum recuperation of 5% of the sample population.

Except for one sample (L03), most of the samples show a high degree of dispersion between single-grain De, suggesting incomplete bleaching. Sample L03 is well-bleached with an overdispersion (OD) of 9.1 ± 5.6% (Appendix B), whereas for rest of the samples solar resetting during deposition was likely incomplete (OD of 21–85 %; Fig. 1). Since the samples were collected from a

flood plain that formed within a graben or pull apart basin, incomplete bleaching is unsurprising (Schielein and Lomax, 2013). A central age model (CAM; Galbraith et al., 1999), therefore, was used only to estimate the burial dose of sample L03 (Appendix B). For the partially bleached samples, we preferred a minimum age model (MAM; Galbraith et al., 1999) using three parameters and assuming a standard OD of 15% in R statistical package for luminescence dating (Kreutzer et al., 2012).

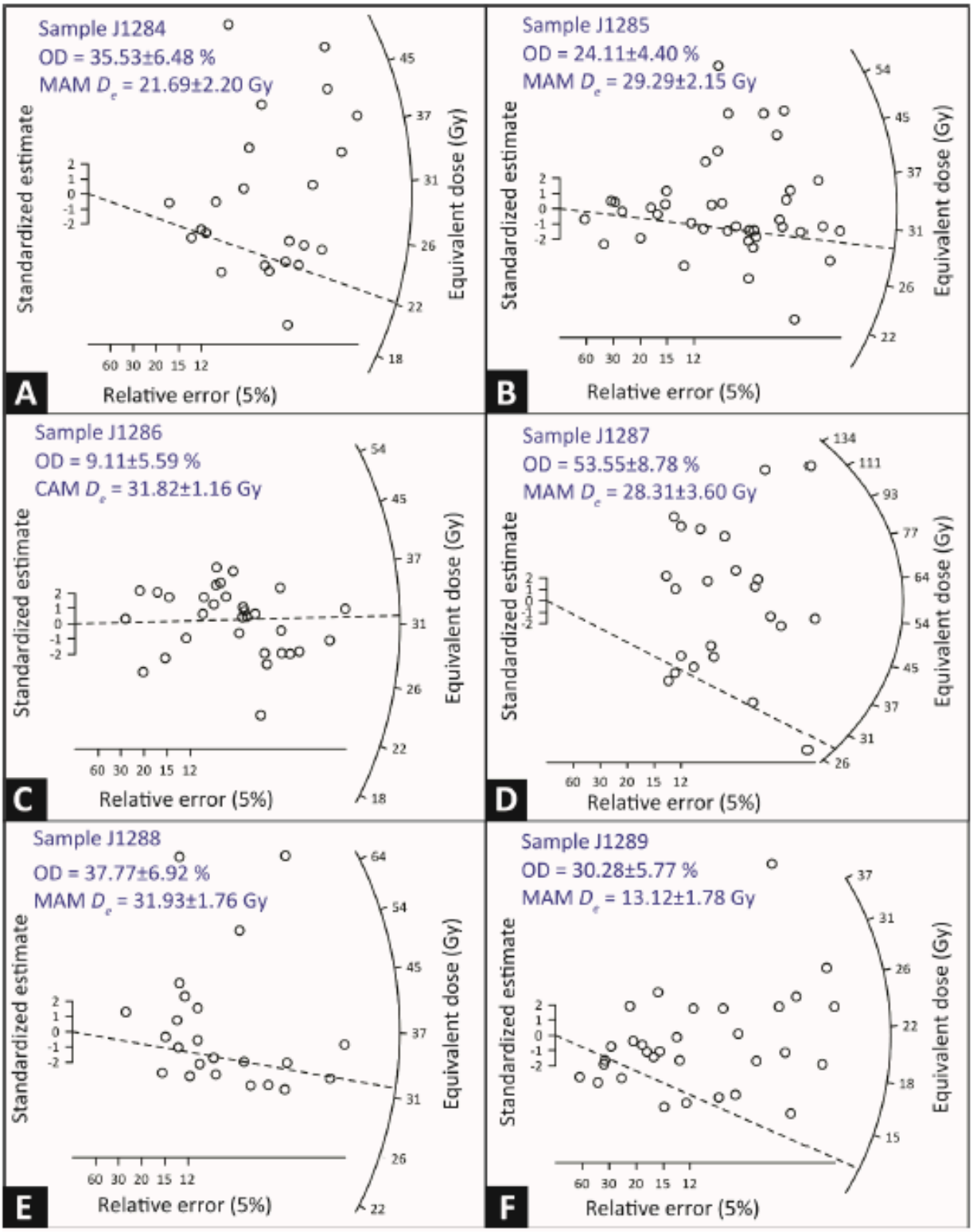
Sample J1284
OD = 35.53±6.48 %
MAM D_e = 21.69±2.20 Gy
Standardized estimate
Equivalent dose (Gy)
Relative error (5%)
A
Sample J1285
OD = 24.11±4.40 %
MAM D_e = 29.29±2.15 Gy
Standardized estimate
Equivalent dose (Gy)
Relative error (5%)
B
Sample J1286
OD = 9.11±5.59 %
CAM D_e = 31.82±1.16 Gy
Standardized estimate
Equivalent dose (Gy)
Relative error (5%)
C
Sample J1287
OD = 53.55±8.78 %
MAM D_e = 28.31±3.60 Gy
Standardized estimate
Equivalent dose (Gy)
Relative error (5%)
D
Sample J1288
OD = 37.77±6.92 %
MAM D_e = 31.93±1.76 Gy
Standardized estimate
Equivalent dose (Gy)
Relative error (5%)
E
Sample J1289
OD = 30.28±5.77 %
MAM D_e = 13.12±1.78 Gy
Standardized estimate
Equivalent dose (Gy)
Relative error (5%)
F

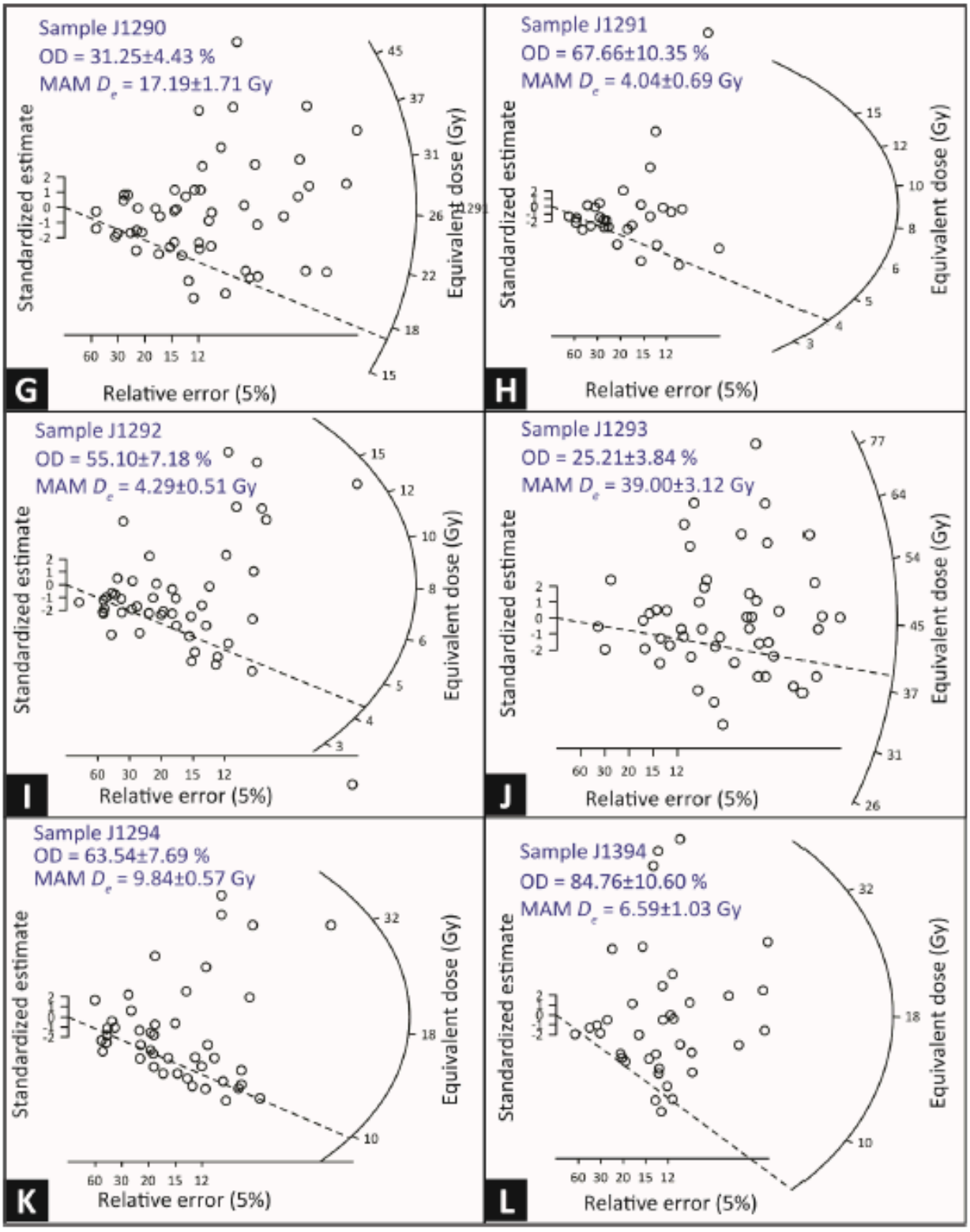
Sample J1290
OD = 31.25±4.43 %
MAM D_e = 17.19±1.71 Gy
Standardized estimate
Equivalent dose (Gy)
Relative error (5%)
G
Sample J1291
OD = 67.66±10.35 %
MAM D_e = 4.04±0.69 Gy
Standardized estimate
Equivalent dose (Gy)
Relative error (5%)
H
Sample J1292
OD = 55.10±7.18 %
MAM D_e = 4.29±0.51 Gy
Standardized estimate
Equivalent dose (Gy)
Relative error (5%)
I
Sample J1293
OD = 25.21±3.84 %
MAM D_e = 39.00±3.12 Gy
Standardized estimate
Equivalent dose (Gy)
Relative error (5%)
J
Sample J1294
OD = 63.54±7.69 %
MAM D_e = 9.84±0.57 Gy
Standardized estimate
Equivalent dose (Gy)
Relative error (5%)
K
Sample J1394
OD = 84.76±10.60 %
MAM D_e = 6.59±1.03 Gy
Standardized estimate
Equivalent dose (Gy)
Relative error (5%)
L

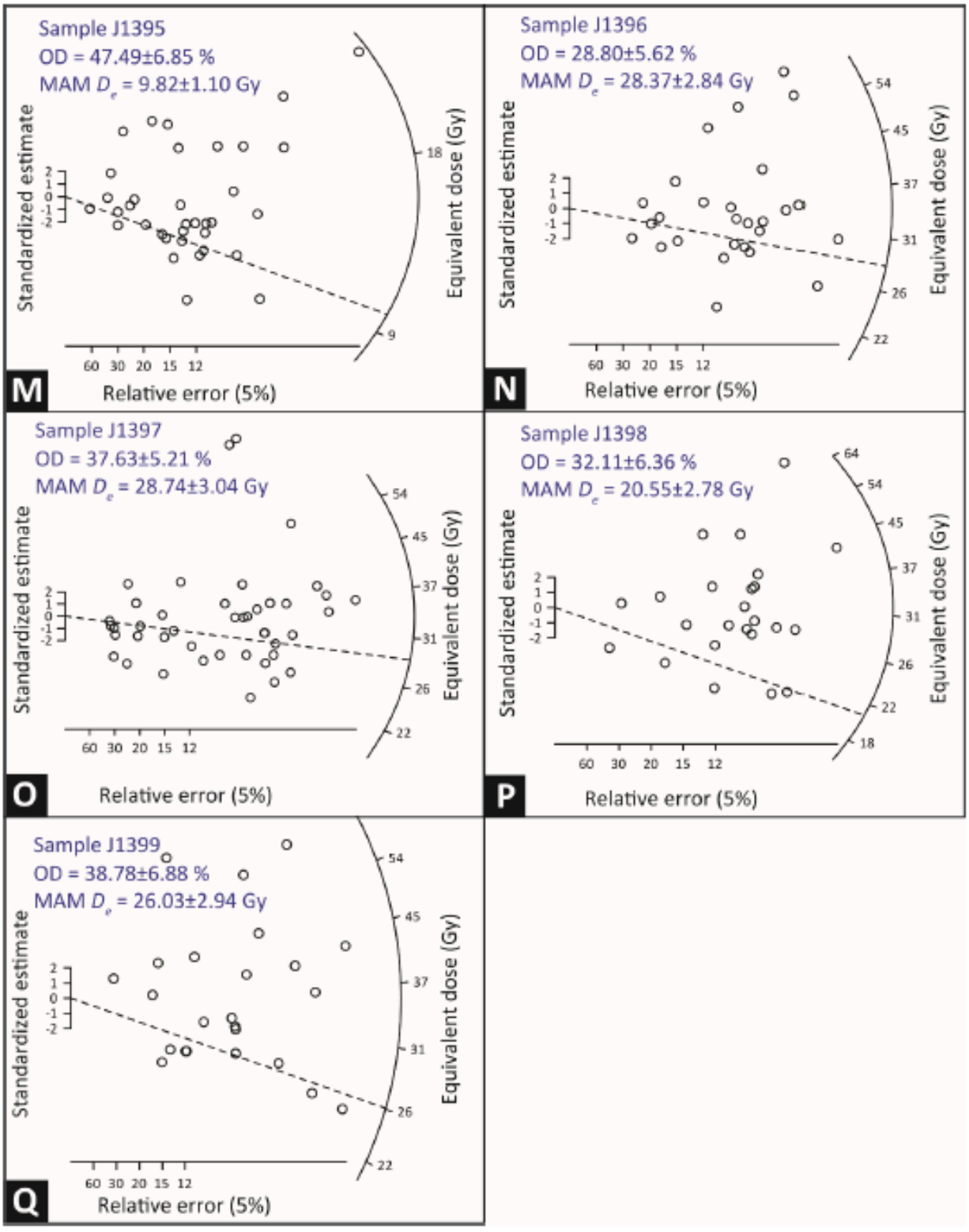
Sample J1395
OD = 47.49±6.85 %
MAM D_e = 9.82±1.10 Gy
Standardized estimate
Equivalent dose (Gy)
Relative error (5%)
M
Sample J1396
OD = 28.80±5.62 %
MAM D_e = 28.37±2.84 Gy
Standardized estimate
Equivalent dose (Gy)
Relative error (5%)
N
Sample J1397
OD = 37.63±5.21 %
MAM D_e = 28.74±3.04 Gy
Standardized estimate
Equivalent dose (Gy)
Relative error (5%)
O
Sample J1398
OD = 32.11±6.36 %
MAM D_e = 20.55±2.78 Gy
Standardized estimate
Equivalent dose (Gy)
Relative error (5%)
P
Sample J1399
OD = 38.78±6.88 %
MAM D_e = 26.03±2.94 Gy
Standardized estimate
Equivalent dose (Gy)
Relative error (5%)
Q

APPENDIX B

TABLE OF EVENT INDICATORS

Event	Wall	Tier	Meter	Evidence and Justification for Quality Rating.	Quality Ranking	Stratigraphic correlation rank	Justification for Stratigraphic Correlation Rating
				Event 1			
E1	West	1	18	Upward fault termination. Correlation between layers across fault was difficult suggesting at least moderate lateral slip.	3	3	This indicator cannot be physically traced to the "secondary type locale" at 9 m on west wall because the event horizon crosses a bench, within an area of discontinuous stratigraphy. The correlation with the secondary type locale is fairly certain, but the secondary type locale is on the opposite wall from the primary type locale and is not near one of the units that has been correlated between walls.
E1	West	2	9	Upward fault termination. Correlation between layers across fault was difficult suggesting significant lateral slip.	3	4	On opposite wall from type locale, but we assume the most recent event on both walls is the same.
E1	West	2	18	Fault with 8 cm vertical seperation that loses visibility between event horizons 1 and 2. There are no clear contacts that prevent the fault from extending up to the event 1 horizon.	2	1	Could be E1 or E2 because the location of the E2 horizon is uncertain in this area and could be located at the upward termination of this fault.
E1	West	1	41	Fault with 12 cm of vertical seperation on layer W208F or W218F extends to within 31 cm from the surface with precise location of termination unclear.	2	1	Could be E1 or E2 because the location of the E2 horizon is uncertain in this area and could be located at the upward termination of this fault.
E1	East	1	20.5	Fault with vertical seperation measured in the tier below (tier 2) is 16 cm on southernmost strand and layers cannot be correlated across the fault suggesting at least moderate lateral slip.	3	4	Event horizon crosses a bench twice between the indicator and the type locale, but correlation is "fairly certain".
E1	East	1	20	Northern strand only has minor offset.	1	4	Event horizon crosses a bench twice between the indicator and the type locale, but correlation is "fairly certain".
E1	East	1	30	Fault that terminates within 24 cm below the event 1 horizon. Offset in event 1 is unknown because stratigraphy could not be correlated. However, in tier 2, vertical seperation is 28 cm potentially accumulated in multiple events.	2	3	The E1 horizon crosses a bench twice and an area of poor stratigraphy between the indicator and the type locale, leading to a somewhat uncertain correlation, but it is still more likely that this indicator correlates with event 1 than with any other recognized event.
E1	East	1	36	Fault with moderate vertical seperation (22 cm?) but upward termination is not distinct. This could be associated with events 1 or 2. The E2 horizon cannot be traced this far south, and the stratigraphy is compressed in this region, such that the E1-E3 horizons may all lie within 30-50 cm of each other.	0	2	The E1 horizon crosses a bench twice and several areas of poor stratigraphy between the indicator and the type locale, leading to a relatively high level of uncertainty, including the possibility that the indicator could correlate with an event other than the proposed event.

E1	East	1	42	Evidence of a fault that clearly offsets δ (purple) layer and could extend very close to the surface. This could potentially be event 1 or event 2. The E2 horizon cannot be traced this far south, and the stratigraphy is compressed in this region, such that the E1-E3 horizons may all lie within 30-50 cm of each other.	0	2	The E1 horizon crosses a bench twice and several areas of poor stratigraphy between the indicator and the type locale, leading to a relatively high level of uncertainty, including the possibility that the indicator could correlate with an event other than the proposed event.
E1	East	1	8	Upward fault termination. Correlation between layers across fault was difficult suggesting at least moderate lateral slip.	4	5	Type section.
E1	East	1	4	Probable fault with minor vertical seperation that terminates within ~20 cm below the event 1 horizon.	2	3	Poor stratigraphy between the indicator and the type locale, which is on the same wall, resulting in a "somewhat uncertain" correlation, but still more likely to be E1 than any other event.
E1	East	2	10	Fault with 28 cm of vertical seperation terminates within ~40 cm below the event 1 horizon.	2	4	Event indicator is across a bench from the type locale, but correlation is "fairly certain".
E1	East	2	9	Fault with minor offset terminates within a few tens of cm below the event 1 horizon.	1	4	Event indicator is across a bench from the type locale, but correlation is "fairly certain".
E1	East	1	16-32	Units E40 through E80 gradually thin and pinch towards against stratigraphy uplifted on south side during event 1.	4	4	Event horizon crosses a bench twice between the indicator and the type locale, but correlation is "fairly certain".
E1	East	2	11	Fault with moderate vertical seperation (24 cm) extends upward to within 32 cm of event 1 horizon.	1	4	Event indicator is across a bench from the type locale, but correlation is "fairly certain".
E1	East	2	12	Fault with minor offset.	1	4	Event indicator is across a bench from the type locale, but correlation is "fairly certain".
				Event2			
E2	West	1	22	Two possible fault strands with minor offset near the base of tier 1 but no clear downward continuation of the fault in tier 2. Upward termination is also unclear, but could be event 2.	0	4	Layer W220E(alpha) is located 0-20 cm below the indicator and can be traced continuously to the type locale. However, the layers above this indicator are discontinuous.
E2	West	3	7	Two fault with minor offset and upward fault termination.	1	2	
E2	West	1	28	Layers W210E and W220E are vertically seperated about 40 cm across a zone of 4 faults. Layer W170E is on top of a scour surface that appears to cap the faults, but earlier logging interpreted this layer as offset. Layer W108E thins and pinches out over this scarp, and definitely caps event 2.	3	5	Type Locale

E2	West	3	14	Fold with 4-5 cm amplitude affects basal layers within the charocal rich silt layer (layer W290). No clear faulting below this fold on the same tier, but there is a fault on tier 4. Top of silt layer does not appear to be folded, but contact is not sharp. A sharp contact marked by green nails is present about 10-15 cm above the top of the layer W290 and is not faulted. The folding could be a a result of liquefaction after event 3, during event 2 or possibly during event 1 or during an aftershock of event 2. Or there could be fault hear that slipped during event 2 fault but died out before reaching the ground surface.	0	2	The event 2 horizon crosses two benches, two faults and areas of discontinuous stratigraphy between the type locale to this indicator, resulting in a relatively high level of uncertainty in exactly where the event 2 horizon should be above this indicator.
E2	East	2	19	Upward fault termination at the based of a scoured channel with moderate offset (12 cm).	3	3	The event 2 horizon on the east wall is only ~30 cm above layer E290, which can be correlated to the west wall of the trench. The correlation is thus somewhat uncertain but there is not other event that this is more likely to correlate with.
E2	East	3	14	Fault with moderate offset of layer E290 stops at bench level in between tiers 2 and 3. Probably slipped in event 2. Poor stratigraphy above fault, could either E1 or E2.	0	1	event 1 horizon. Correlation of E290 between east and west walls is strong (4); correlation of event 1 horizon between east and west walls moderate (3)
				Event 3			
E3	West	2 & 3	6-14m (T3); 16-18 (T2)	We interpret that fault scarps that were formed during event 3 down dropped blocks to the north creating a closed depression where water flowed and came to a halt depositing very fine grained material (charcoal rich silt).	3	5	Type Locale
E3	East	3	12-20m	Silt layer E290 is thickest in area where units are down dropped the most between faults. Layer E290 appears to thin out towards the south but the exact location of the pinch out is not clear.	1	4	Layer 290 can be correlated between the two walls with a high degree of certainty based on is thickness, grain size and presence of abundant charcoal.
E3	East	2	27	Fault with minor displacement terminates within tier 2, and is capped by a contact that could potentially be the base of a debris flow which may correlate the event 3 horizon to the north.	1	1	Layer 290 does not exist this far south, and our preferred interpretation of where it would be is uncertain. Stratigraphic distance between the E2 and E3 horizons here is < 0.5 m, making it hard to rule out the possibility that this indicator could have formed during event 2.
E3	East	3	19	Fault with major vertical seperation that is visible to the top of tier 3 but not visible in tier 2. The event 3 horizon lies at the base of tier 2, so this fault probably ruptured during event 3.	2	4	These faults are potentially capped but E290 which can be correlated to W290 with a high degree of certainty.

E3	East	3	18	Fault with major vertical seperation that may extend to the top of tier 3 but Is not visible in tier 2. Probably slipped in event 3.	2	4	These faults are potentially capped but E290 which can be correlated to W290 with a high degree of certainty.
				Event 4			
E4	West	1	32	In the dugout 30-32 m in Tier 1, a fault with moderate vertical seperation of a layer nailed purple-white and is capped by a scour nailed double green that formed at the base of a sandy channel. Quality ranking is 2 because it is not clear whether the sharp scour contact is present across the fault zone.	2	5	Type Locale
E4	West	2	23	Fault with moderate offset (~6 cm) of vertical seperation capped by layer W390.	2	3	The event 4 horizon lies at the base of Layer W390C which can be well traced throughout tier 2 but jumps a fault and a bench onto tier 1. On Tier 1, layer W390C cannot be located with certainty. Because of this, the correlation to the type locale is somewhat uncertain.
E4	West	2	22	Upward fault termination with moderate offset, but no clear location on the upward termination of the fault. Fault could be capped by layer W470C or could continue onto base of tier 2 and be capped by the event 4 horizon.	0	3	The event 4 horizon lies at the base of Layer W390C which can be well traced throughout tier 2 but jumps a fault and a bench onto tier 1. On Tier 1, layer W390C cannot be located with certainty. Because of this, the correlation to the type locale is somewhat uncertain.
E4	East	2	32	Fault terminates upward with minor offset.	1	2	This event indicator is located above one of our correlable layers (E610) and is on the same tier as layer E610 but it is unclear at whether stratigraphic horizon at which this event indicator terminates is the same exact horizon as event 4 at the type locale on the opposite wall. The indicator is not bracketed beween two correlable layers, because location of layuer E290 is unclear. While our prefered interpretaion is event 4, we cannot fully rule out the possibility it can be event 5 (or event 3). Therefore, the stratigraphic correlation has a high level of uncertainty.
E4	East	2	36	Fault terminates upward with minor offset.	1	2	" "
E4	East	3	24	A fault with minor offset originally mapped as capped by unit E480, but may extend upward and correlate with a fault in tier 2. Could potentially be event 3 or 4.	1	2	This event indicator is located above one of our correlable layers (E610), but is not bracketed beween two correlable layers, because location of layer E290 is unclear. While our prefered interpretaion is event 4, we cannot fully rule out the possibility it can be event 3. Therefore, the stratigraphic correlation has a high level of uncertainty.

				Event 5			
E5	West	1	50	4 faults with minor vertical seperation of layer W590D capped by W490D. Total veritcal seperation across the zone is ~ 10 cm. Therefore, we consider this moderate offset. Upward termination is indistinct, but there is a sharp capping layer about 30 cm above the faults. Our preferred interpretation is that this is a younger event than event 6, but we cannot rule out whether this indicator could have formed during event 6.	2	4	Type Locale. Our preferred interpretation is that this is a younger event than event 6, but we cannot rule out whether this indicator could have formed during event 6. Therefore we assign correlation rating of 4 instead 5 for the type locale.
E5	East	2	32	Fault splay with very minor offset gets capped by layer E440.	0	3	At this event indicator we are fairly certain that the event indicator lies above layer E610(the top of this layer is the E6 horizon) and below the event 4 indcator. The only uncertainty here, is that the type locale is on the opposite wall.
E5	East	3	26	Minor offset on a faults that downdrops debris flow layer E520 into a small graben that is capped by muddy silt layer E490.	1	3	This event indicator lies < 1 m above layer E610. We cannot see where the event 4 horizon lies above this event indicator, which causes some uncertainty. Our preferred interpretation is that this event indicator is at the event 5 horizon.
E5	East	3	24	Fault with minor offset.	1	3	" "
E5	East	3	25	Fault with minor offset.	1	3	" "
E5	East	3	23	A fracture in layer E520 that is weathering out and may connect downward to a fault. Better than a 0 because there is a distinct upward termination but not a 1 because there is no measureable offset.	0.5	3	" "
				Event 6			
E6	East	3	22-27	Layers E520 and E525 thin from 60 cm at 23 m to 20 cm at 26 m. Note: cannot be linked to a causitive fault.	3	5	Type Locale
E6	West	2	38	Minor vertical seperation of layer W604C (~ 2 cm) capped by layer W590C.	1	2	The E6 horizon lies above one of our correlable layers (610). This event indicator is above layer 610 but the location of the E5 horizon above this event indicator is uncertain and correlation of the event 6 horizon across the fault at 32 m is very uncertain. This allows the possibility that this indicator could of formed in a different event.
E6	West	2	39	Minor vertical seperation of layer W604C (~ 2 cm) capped by layer W590C.	1	2	The E6 horizon lies above one of our correlable layers (610). This event indicator is above layer 610 but the location of the E5 horizon above this event indicator is uncertain and correlation of the event 6 horizon across the fault at 32 m is very uncertain. This allows the possibility that this indicator could of formed in a different event.

E6	West	4	23	A fault with minor vertical seperation capped by layer W590.	1	4	This event horizon is just above layer 610, which can be correlated between the two walls. It is also well below the interpreted position of the event 5 horizon.
E6	West	4	23	A faults with minor vertical seperation capped by layer W590.	1	4	This event horizon is just above layer 610, which can be correlated between the two walls. It is also well below the interpreted position of the event 5 horizon.
				Event 7			
E7	East	3	36	Fault with 5 cm vertical separation in upper part of tier 4 (pebble layer E710) is capped by an unfaulted fine sand layer (E690) at base of tier 3. We did not dig this out, so we never saw the fault and the capping layer on the same tier.	2	4	The fine sand layer (E690) that caps this indicator can be correlated with a fair degree of certainty across one fault from the type locale.
E7	East	4	32	An 80-cm-thick package of very fine sand, silt and clay (E660-E690) thins to 10-15 cm (E690) across a fault and then pinches out to south. The causative fault has re-ruptured in younger earthquakes.	3	5	Type Locale.
E7	West	4	28	Layer W690 thins to the south and pinches out but there is no clear casuative fault.	1	2	The fine sand layer that caps this indicator (W690) is below W610 and above W850, both of which can be correlated to the opposite wall of the trench. However, it is not particularly close to either of these correleable layers, so it is hard to tell for certain whether this capping layer correlates with E690 at the type locale.
				Event 8			
E8	East	4	36	Layers E780 and E790 thin and pinch out to the south. We interpret this as growth strata. The causitive fault (34 m) has 40 cm of vertical seperation on layer E840B (below the growth strata) but only 5 cm of vertical seperation on layer E710 above the growth strata.	2	2	This indicator and the type locale are both probably above unit 850, but that unit cannot be phyically traced to either of these indicators.
E8	West	4	32	Fault with moderate vertical seperation (22 cm) of layer W815-W815B. Capped by layer of fine sand (layer W790C).	2	3	Fine sand layer capping this indicator (W790C) probably correlates with unit W790 capping the type locale, but there is some uncertainty due to crossing and area of poor stratigraphy and crossing a fault.
E8	West	4	36	Fine sand layer W790C thins towards the south and pinches out against a fault.	2	5	Type Locale

APPENDIX C

EARTHQUAKE CHRONOLOGY USING AN ALTERNATIVE AGE MODEL

Our preferred interpretation of the radiocarbon and luminescence ages omitted any radiocarbon ages that were older that other samples from the same or lower units. Here we present an alternate model that uses seven radiocarbon dates and sixteen IRSL samples to constrain the ages of our eight paleoearthquakes (Figure C1). Unlike our preferred model, this alternate model includes some of the older radiocarbon samples (e.g., A33, A39 and A35 at 2.6-2.9 m stratigraphic depth) and assumes that the youngest sample (A18) from that depth range (which is 2000-years younger) does not accurately represent the age of these strata, perhaps due to unrecognized bioturbation. Furthermore, we decided to keep IRSL samples L19 and L05 and instead omit sample L07, to explore the effects of samples choices that reflect an alternate end member to our preferred model. Based on this alternate model, we observe that the paleoearthquake ages are unchanged for events 1, 2, 3, 7 and 8. Events 4 and 5 have a age difference of ~2000 years between the two models, while event 6 has a similar maximum age in both models (~5100 years) but a different, minimum age in the two models (3350 versus 4890 years). The sample ages in the alternate model also display a 2000-year depositional haitus between events 3 and 4.

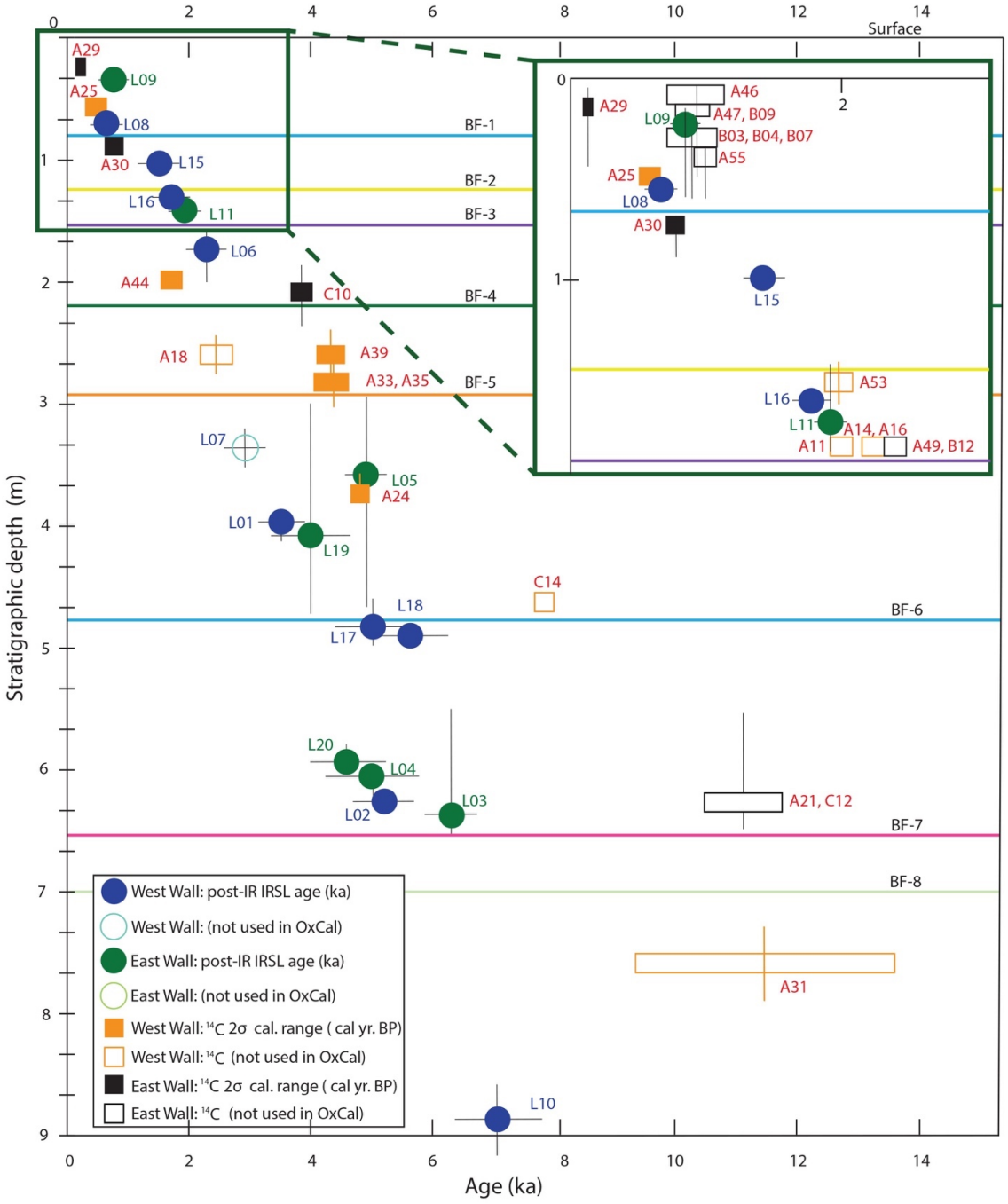

Figure C1: *Calibrated radiocarbon and post-IR IRSL ages as a function of stratigraphic depth. Stratigraphic depth was measured on the west wall at 24 m (for layers 20 - 620) and at 34 m (for layers 620 - 850). Vertical error bars show uncertainties in correlating sample locations from the east wall or from other fault blocks on the west wall with the type section. Solid symbols show ages that were included in our alternate OxCal model; open symbols show samples excluded from that model.*

Table C1. Ages of radiocarbon (R_Date) and luminescence (C_Date) samples and paleoearthquakes.

	Unmodeled (BC/AD)			Modelled (BC/AD)			BP	
	from	to	%	from	to	%	from	to
Boundary Surface				1527	2278	95.4		
R_Date A29	1522	…	95.4	1516	1953	95.3	434	-3
C_Date L09	895	1315	95.4	1281	1438	95.4	669	512
R_Date A25	1276	1390	95.4	1273	1385	95.4	677	565
C_Date L08	996	1488	95.4	1083	1333	95.4	867	617
E1				1010	1258	95.4	940	692
R_Date A30	987	1149	95.4	985	1121	95.4	965	829
C_Date L15	167	1030	95.4	471	1017	95.4	1479	933
E2				285	869	95.4	1665	1081
L16	-128	700	95.4	195	600	95.4	1755	1350
L11	-193	315	95.4	143	402	95.4	1807	1548
E3				109	339	95.4	1841	1611
C_Date L06	-1000	286	95.4	87	267	95.4	1863	1683
R_Date A44	87	238	95.4	77	208	95.4	1873	1742
R_Date C10	-2130	-1926	95.4	-2124	-1925	95.4	4074	3875
E4				-2352	-1976	95.4	4302	3926
R_Date A39	-2469	-2212	95.4	-2436	-2206	95.4	4386	4156
R_Date A35	-2576	-2467	95.4	-2573	-2466	95.4	4523	4416
R_Date A33	-2457	-2150	95.4	-2466	-2246	95.4	4416	4196
E5				-2816	-2481	95.4	4766	4431
C_Date L05	-3698	-2428	95.4	-2929	-2559	95.4	4879	4509
C_Date L19	-3219	-968	95.4	-2997	-2655	95.4	4947	4605
R_Date A24	-3086	-2890	95.4	-3022	-2889	95.4	4972	4839
C_Date L01	-2427	-894	95.4	-3150	-2900	95.4	5100	4850
E6				-3397	-2927	95.4	5347	4877
C_Date L17	-4270	-2118	95.4	-3572	-2987	95.4	5522	4937
C_Date L18	-4993	-2482	95.4	-3742	-3070	95.4	5692	5020
C_Date L20	-4116	-1816	95.4	-3891	-3163	95.4	5841	5113
C_Date L04	-4564	-1860	95.4	-4069	-3281	95.4	6019	5231
C_Date L02	-4271	-2550	95.4	-4268	-3434	95.4	6218	5384
C_Date L03	-4999	-3739	95.4	-4603	-3675	95.4	6553	5625
E7				-4941	-3775	95.4	6891	5725
E8				-5238	-3899	95.4	7188	5849
C_Date L10	-6301	-3877	95.4	-5521	-4033	95.4	7471	5983
Boundary Base				-5824	-4108	95.4	7774	6058

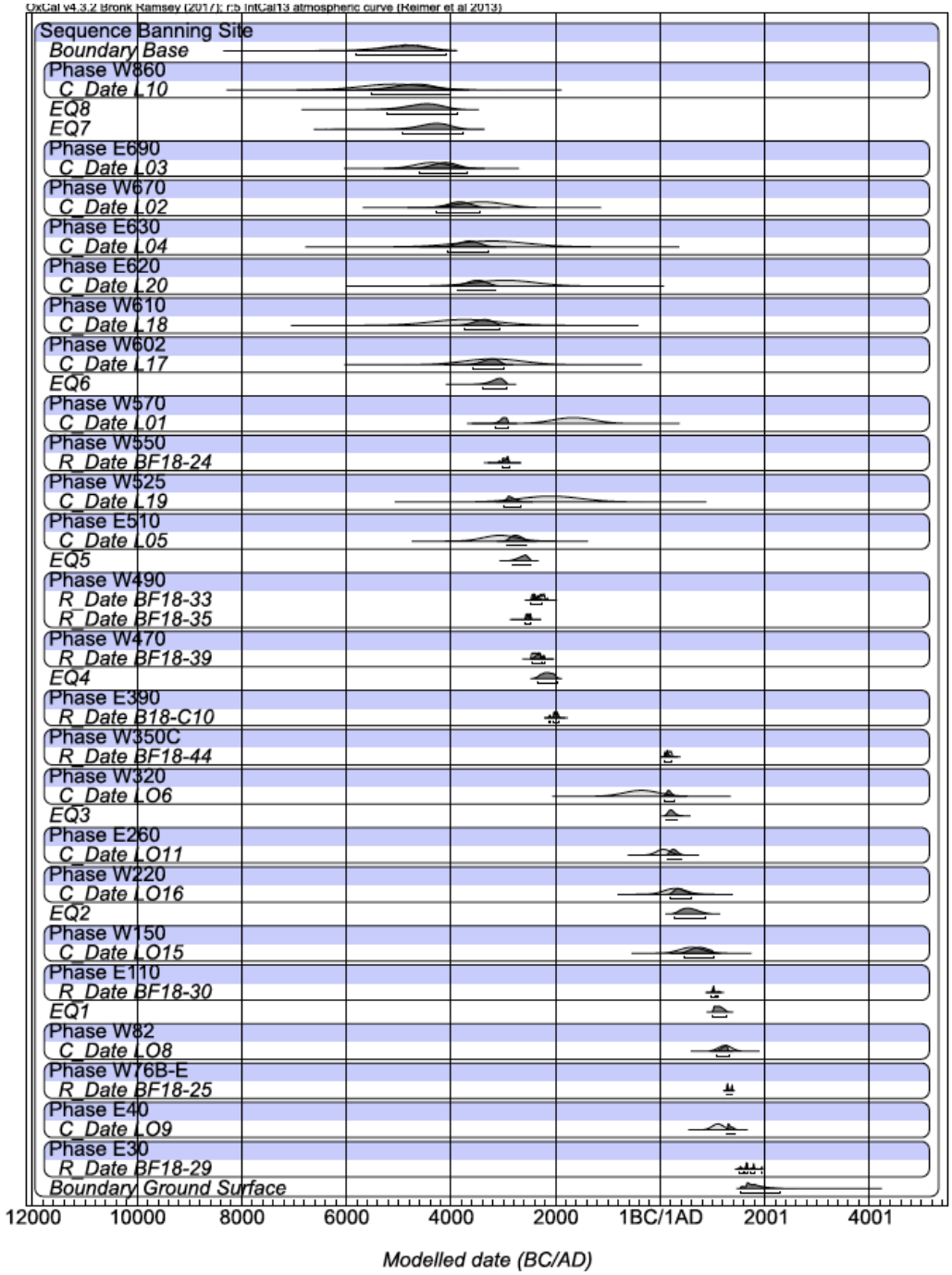

Figure C2: *Ages from the 18th Avenue trench that were used in the OxCal model to estimate earthquake ages. Ages are plotted as a function of stratigraphic position. Curves shaded light grade are the a priori probability density functions obtained for the ages of individual samples. Curves shaded in dark gray are the posterior probability density functions for each sample. In the Bayesian approach used within OxCal, the ages of samples above and below a given sample are used to reweight the probability density function for that sample so as to yield a set of ages that are stratigraphically consistent with each other as well as being consistent with the a priori (measured) ages of each sample.*

REFERENCES

Allen, C. R., 1957, San Andreas Fault zone in San Gorgonio Pass, Southern California: Geological Society of America Bulletin, Vol. 68, pp. 315-350.

Behr, W.M., Rood, D.H., Fletcher, K.E., Guzman, N., Finkel, R., Hanks, T.C., Hudnut, K.W., Kendrick, K.J., Platt, J.P., Sharp, W.D., Weldon, R.J., and Yule, J.D., 2010, Uncertainties in slip-rate estimates for the Mission Creek strand of the southern San Andreas Fault at Biskra Palms Oasis, southern California: Geological Society of America Bulletin, v. 122, p. 1360-1377, doi:10.1130/B30020.1.

Biasi, G. P., Weldon, Ray J., II, Fumal, T. E., & Seitz, G. G. 2002, Paleoseismic event dating and the conditional probability of large earthquakes on the southern San Andreas fault, California: Bulletin of the Seismological Society of America, 92(7), 2761-2781. doi:10.1785/0120000605.

Blisniuk, K. D., Scharer, K., Burgmann, R., Sharp, W., Rymer, M., Rockwell, T., and Williams, P., 2012, A new slip rate estimate for the San Andreas fault zone in the Coachella Valley at Pushawalla Canyon, California: Southern California Earthquake Center 2012 Annual Meeting, Abstract #129.

Blisniuk, K. D., Scharer K., Sharp W. D., Burgmann R., Rymer M.J., and Williams P., 2013, New geological slip rate estimates for the Mission Creek strand of the San Andreas fault zone: Southern California Earthquake Center 2013 Annual Meeting, Abstract #032.

Bonilla, M. G., and Lienkaemper, J. J. 1991, Factors affecting the recognition of faults exposed in exploratory trenches. U.S.Geological Survey Bulletin,54.

Bøtter-Jensen, L., Andersen, C., Duller, G., Murray, A., 2003, Developments in radiation, stimulation and observation facilities in luminescence measurements. Radiation Measurements 37, 535–541.

Brennan, B.J., Lyons, R.G., Phillips, S.W., 1991, Attenuation of alpha particle track dose for spherical grains. Int. J. Radiat. Appl. Instrum. Part D. Nucl. Tracks Radiat. Meas. 18, 249–253.

Bronk Ramsey, C., 2009, Bayesian Analysis of Radiocarbon Dates: Radiocarbon, v. 51, p. 337–360, doi: 10.1017/S0033822200033865.

Buylaert, J., Murray, A., Thomsen, K., Jain, M., 2009, Testing the potential of an elevated temperature IRSL signal from K-feldspar. Radiation Measurements 44, 560–565.

Cardona, J., 2016, Constraining the most recent surface rupture on the Garnet Hill strand, San Andreas Fault, Coachella Valley, California [Master's Thesis]: Northridge, California State University.

Durcan J. A., King G. E., Duller GAT. 2015, DRAC: Dose Rate and Age Calculator for trapped charge dating. Quaternary Geochronology 28: 54–61.

Fletcher, K.E.K., Sharp, W.D., Kendrick, K.J., Behr, W.M., Hudnut, K.W., and Hanks, T.C., 2010, 230Th/U dating of a late Pleistocene alluvial fan along

the southern San Andreas fault: Geological Society of America Bulletin, v. 122, p. 1347-1359, doi:10.1130/B30018.1.

Fumal, T.E., Pezzopane, S.K., Weldon, R.J., Schwartz, D.P., 1993, A 100-year Average Recurrence Interval for the San Andreas Fault at Wrightwood, California: Science, v. 259, i. 5092, p.199-203.

Fumal T. E., M. J. Rymer, G. G. Seitz, 2002a, Timing of Large Earthquakes since A.D. 800 on the Mission Creek Strand of the San Andreas Fault Zone at Thousand Palms Oasis, near Palm Springs, California: Bulletin of the Seismological Society of America, Vol. 92, No. 7, pp. 2841-2860.

Fumal, T. E., Weldon, R J, II, Biasi, G P, Dawson, T E, Seitz, G G; et al., 2002b, Evidence for large earthquakes on the San Andreas Fault at the Wrightwood, California, paleoseismic site; A.D. 500 to present, Bulletin of the Seismological Society of America, 92.7, p. 2726-2760.

Galbraith, R.F., Roberts, R.G., Laslett, G.M., Yoshida, H., Olley, J.M., 1999, Optical dating of single and multiple grains of quartz from Jinmium rock shelter, northern Australia: Part I, experimental design and statistical models. Archaeometry 41, 339–364.

Gold, P. O., Behr, W. M., Rood, D., Kendrick, K., Rockwell, T. K. and Sharp, W. D., 2015, Holocene geologic slip rate for the Banning strand of the southern San Andreas Fault near San Gorgonio Pass: Journal of Geophysical Research B: Solid Earth, v. 120, no. 8, p.5639-5663.

Guerin, G., Mercier, N., Nathan, R., Adamiec, C., Lefrais, Y., 2012, On the use of the infinite matrix assumption and associated concepts: a critical review. Radiat. Meas. 47, 778–785.

Harden, J. W., and Matti, J. C., 1989, Holocene and late Pleistocene slip rates on the San Andreas fault in Yucaipa, California, using displaced alluvial-fan deposits and soil chronology. Geological Society of America Bulletin, 101(9), 1107-1117. doi:2.3.CO;2.

Huntley, D.J., Baril, M.R., 1997, The K content of the K-feldspars being measured in optical dating or in thermoluminescence dating. Anc. TL 15, 11–13.

Huntley, D.J., and Lamothe, M., 2001, Ubiquity of anomalous fading in K-feldspars and the measurement and correction for it in optical dating. Canadian Journal of Earth Sciences 38, 1093–1106.

Kreutzer, S., Schmidt, C., Fuchs, M., Dietze, M., Fischer, M., Fuchs, M., 2012, Introducing an R package for luminescence dating analysis. Ancient TL 30, 1–8.

Lienkaemper, J. J., and Ramsey, C. B., 2009, OxCal; versatile tool for developing paleoearthquake chronologies; a primer. Seismological Research Letters, 80(3), 431-434.

Liritzis, I., Stamoulis, K., Papachristodoulou, C., Ioannides, K., 2013, A re-evaluation of radiation dose rate conversion factors. Mediterr. Archaeol. Archaeom. 13, 1–15.

Matti, J.C., and Morton, D.M., 1993, Paleogeographic evolution of the San Andreas fault in southern California: A reconstruction based on a new cross-fault correlation, in Powell, R.E., Weldon, R.E., II, and Matti, J.C., eds., The San Andreas fault system: Displacement, palinspastic reconstruction, and geologic evolution: Geological Society of America Memoir 178, p. 107–159.

McCaffrey, R., 2005, Block Kinematics of the Pacific-North America Plate Boundary in the Southwestern United States from Inversion of GPS, Seismological, and Geologic data, J. Geophys. Res., 110, B07401, doi:10.1029/2004JB003307.

McGill, S. F., and Rubin, C. M., 1999, Surficial slip distribution on the central Emerson fault during the June 28, 1992, Landers Earthquake, California. Journal of Geophysical Research, 104, 4811-4833. doi: /10.1029/98JB01556.

McGill, S.F., Dergham, S., Barton, K., Berney-Ficklin, T., Grant, D., Hartling, C., Hobart, K., McCGill, J., Minnich, R., Rodriguez, M., Russell, J., Schmoker, K., Stumfall, M., Townsend, J., Williams, J., 2002, Paleoseismology of the San Andreas fault at Plunge Creek, near San Bernardino, southern California: Bulletin of Seismological Society of America, v. 92, p. 2803-2840.

McGill, S., Owen, L., Weldon, R. J., and Kendrick, K., 2013, Latest Pleistocene and Holocene slip rate for the San Bernardino strand of the San Andreas

fault, Plunge Creek, Southern California: Implications for strain partitioning within the southern San Andreas fault system for the last ~35 k.y.: Geological Society of America Bulletin, v. 125, no. 1/2, p. 48-72, doi: 10.1130/B30647.1.

McGill, S. F., Spinler J.C., McGill J. D., Bennett R. A., Floyd M., Fryxell J. E., and Funning G.J., 2015, Kinematic modeling of fault slip rates using new geodetic velocities from a transect across the Pacific-North America plate boundary through the San Bernardino Mountains, California, Journal of Geophysical Research, v. 120, p. 2772–2793, 10.1002/2014JB011459.

Meade, B. J., and Hager, B. H., 2005, Block models of crustal motion in southern California constrained by GPS measurements, Journal of Geophysical Research, 110, B03403, doi:10.1029/2004JB003209.

Nicholson, C.,1996, Seismic behavior of the southern San Andreas fault zone in the Northern Coachella Valley, California; comparison of the 1948 and 1986 earthquake sequences. Bulletin of the Seismological Society of America, 86(5), 1331-1349.

Nur, A., Ron H., and Beroza G. C., 1993, The Nature of the Landers-Mojave Earthquake Line, Science, 261, 5118, 201–203.

Orozco, A.A., 2004, Offset of a mid-Holocene alluvial fan near Banning, CA; constraints on the slip rate of the San Bernardino strand of the San Andreas fault [Master's Thesis]: Northridge, California State University.

Orozco, A., and Yule, D., 2003, Late Holocene slip rate for the San Bernardino strand of the San Andreas fault near Banning, California. Seismological Research Letters, 74(2), 237.

Philbosian, B., Fumal, T.E., and Weldon, R.J., 2011, San Andreas Fault earthquake chronology and Lake Cahuilla history at Coachella, California: Bulletin of the Seismological Society of America, v. 101(1), p. 13-38.

Prescott, J. R., and Hutton J.T., 1994, Cosmic ray contributions to dose rates for luminescence and ESR dating: large depths and long-term time variations. Radiation Measurements 23, 497–500.

Reimer, P.J., Bard, E., Bayliss, A., Beck, J.W., Blackwell, P.G., Ramsey, C.B., Buck, C.E., Cheng, H., Edwards, R.L., Friedrich, M., Grootes, P.M., Guilderson, T.P., Haflidason, H., Hajdas, I., et al., 2013, IntCal13 and Marine13 Radiocarbon Age Calibration Curves 0–50,000 Years cal BP: Radiocarbon, v. 55, p. 1869–1887, doi: 10.2458/azu_js_rc.55.16947.

Rhodes, E., 2015, Dating sediments using potassium feldspar single-grain IRSL: initial methodological considerations. Quaternary International 362, 14–22.

Rockwell, T. K., Meltzner, A. J., and Haaker, E. C., 2018, Dates of the two most recent surface ruptures on the southernmost San Andreas Fault recalculated by precise dating of lake Cahuilla dry periods. *Bulletin of the Seismological Society of America, 108*(5), 2634-2649. doi:http://dx.doi.org/10.1785/0120170392.

Rymer, M. J., 1997, Structural Link Between the San Andreas Fault and the Eastern California Shear Zone, Coachella Valley and Little San Bernardino Mountains, Southern California, Geol. Soc. Am., Abstr. Programs, 29(5), 61–62.

Scharer, K., R. Weldon II, Biasi G., Streig A., and Fumal T., 2017, Ground-rupturing earthquakes on the northern Big Bend of the San Andreas Fault, California, 800 A.D. to Present, J. Geophys. Res. Solid Earth, 122, 2193–2218 doi:10.1002/2016JB013606.

Scharer, K., Blisniuk, K., Sharp, W., and Mudd, S. M., 2016, Slip transfer and the growth of the Indio and Edom Hills, southern San Andreas fault. Abstracts with Programs - Geological Society of America, 48(4), Abstract no. 14-3. doi:/10.1130/abs/2016CD-274217.

Scharer, K. M., Yule, D., Humbert, L. R., and Witkowsky, R., 2013, Implications for San Andreas fault ruptures based on new evidence from the Cabazon, CA paleoseismic site, San Gorgonio pass fault zone. American Geophysical Union Fall Meeting, 2013, Abstract T43A-2622.

Scharer, K. M., Biasi G.P., and Weldon R.J., 2011, A reevaluation of the Pallett Creek Earthquake Chronology Based on New AMS Radiocarbon Dates, San Andreas fault, California, J. Geophys. Res., 116, B12111, doi:10.1029/2010JB008099.

Schielein, P., and Lomax, J., 2013, The effect of fluvial environments on sediment bleaching and Holocene luminescence ages – A case study from the German alpine foreland. Geochronometria 40, 283– 293.

Seitz, G.G., Weldon, R. II., and Biasi, G.P., 1997, The Pitman Canyon paleoseismic record; a re-evaluation of southern San Andreas Fault segmentation: Journal of Geodynamics, v. 24, no.1-4, p. 129-138.

Sharp, R.V., Rymer, M.J., and Morton, D.M., 1986, Trace-fractures on the Banning fault created in association with the 1986 North Palm Springs earthquake, Bulletin of the Seismological Society of America, v. 76, p. 1837-1843.

Sieh, K. E., and Williams P.L., 1990, Behavior of the southernmost San Andreas fault during the past 300 years, J. Geophys. Res. 95, 6629-6645.

Spinler, J.C., Bennett, R.A., Anderson, M.L., McGill, S.F., Hreinsdóttir, S., and McCallister, A., 2010, Present-day strain accumulation and slip rates associated with southern San Andreas and Eastern California shear zone faults: Journal of Geophysical Research, v. 115, p. B11407, doi:10.1029/2010JB007424.

Stuiver, M., & Polach, H., 1977, Discussion: Reporting of 14C Data. Radiocarbon, 19, 355- 363.

U.S. Geological Survey and California Geological Survey, 2006, Quaternary fault and fold database for the United States, accessed December 15, 2015, from USGS web site: http//earthquake.usgs.gov/hazards/qfaults/.

Van der Woerd, J., Klinger, Y., Sieh, K., Tapponnier, P., Ryerson, F. J., and Meriaux, A., 2006, Long-term slip rate of the southern San Andreas fault from (super 10) be- (super 26) al surface exposure dating of an offset alluvial fan. Journal of Geophysical Research, 111, 17. doi:/10.1029/2005JB003559.

Weldon, R.J.II, Fumal, T.E., Powers, T.J., Pezzopane, S.K., Scharer, K.M., and Hamilton, J.C., 2002, Structure and earthquake offsets on the San Andreas Faults at the Wrightwood, California paleoseismic site, Bull. Seismo. Soc. Am. 92; no. 7, 2704-2725.

Weldon, R. J., and Sieh, K.E., 1985, Holocene rate of slip and tentative recurrence interval for large earthquakes on the San Andreas fault, Cajon Pass, southern California: Geological Society of America Bulletin, v. 96, p. 793-812.

Williams, P. L., McGill S.F., Sieh K. E., Allen C. R., and Louie J.N., 1988, Triggered slip along the San Andreas fault after the 8 July 1986 North Palm Springs earthquake, Bulletin of the Seismological Society of America, v. 78, pp. 1112-1122, 1988.

Wintle, A., and Murray, A., 2006, A review of quartz optically stimulated luminescence characteristics and their relevance in single-aliquot regeneration dating protocols. Radiation Measurements 41, 369– 391.

Wolff, L. R., and Yule, D., 2014, Reconciling contradicting trench and geomorphologic observations across the San Gorgonio Pass Fault Zone:

Southern California Earthquake Center 2014 Annual Meeting, Abstract #282.

Yule, D., and Sieh, K., 2003, Complexities of the San Andreas fault near San Gorgonio Pass: Implications for large earthquakes: Journal of Geophysical Research, v. 108, no. B11, ETG 9-1–9-23, doi: 10.1029/2001JB000451.

Yule, J., Fumal, T., McGill, S., and Seitz, G., 2001, Active tectonics and paleoseismic record of the San Andreas fault, Wrightwood to Indio: Working toward a forecast of the next “Big Event”, in Dunne, G., and Cooper, J., eds., Geologic excursions in the Californian deserts and adjacent Transverse Ranges: Los Angeles, California, Pacific Section, SEPM, p. 91-126.

Yule, D., Seih, K., Weigand, P. W., and Shellebarger, J., 2001, The paleoseismic record at Burro Flats; evidence for a 300-year average recurrence for large earthquakes on the San Andreas fault in San Gorgonio pass, southern California. Abstracts with Programs - Geological Society of America, 33(3), 31.

Yule, J. D., Maloney, S. J., Cummings, L. S., Prentice, C., Ellsworth, W., and Hellweg, P., 2006, Using pollen to constrain the age of the youngest rupture of the San Andreas fault at San Gorgonio Pass. Seismological Research Letters, 77(2), 245.